ORIGINAL PAPER

Biological Applications, In Vitro Cytotoxicity, Cellular Uptake, and Apoptotic Pathway Studies Induced by Ternary Cu (II) Complexes Involving Triflupromazine with Biorelevant Ligands

Nourhan S. Sultan[1] · Azza A. Shoukry[2] · Fatma B. Rashidi[3] · Heba K. A. Elhakim[3]

Abstract

The novel mixed-ligand complexes derived from the parent antidepressant phenothiazine drug triflupromazine (TFP) were synthesized along with the secondary ligands glycine and histidine. [Cu(TFP)(Gly)Cl]·2H$_2$O (**1**) and [Cu(TFP)(His) Cl]·2H$_2$O (**2**) were examined for their in vitro biological properties. Cyclic voltammetry was used to study the binding of both complexes to CT-DNA. The two complexes were examined for antiviral, antiparasite, and anti-inflammatory applications. An in vitro cytotoxicity study on two different cancer cell lines, MCF-7, HepG2, and a normal cell line, HSF, shows promising selective cytotoxicity for cancer cells. An investigation of the cell cycle and apoptosis rates was evaluated by flow cytometry with Annexin V-FITC/Propidium Iodide (PI) staining of the treated cells. Gene expression and western blotting were carried out to determine the expression levels of the pro-apoptotic markers and the anti-apoptotic marker Bcl2. The tested complexes decreased cell viability and triggered apoptosis in human tumor cell lines. Molecular docking was also used to simulate Bcl2 inhibition. Finally, complex (**2**) has potent antitumor effects on human tumor cells, especially against HepG2 cells, as seen in the cellular drug uptake assay. Consequently, complex (**2**) may prove useful against cancer, especially liver cancer. For further understanding, it needs to be explored in vivo.

Graphical Abstract
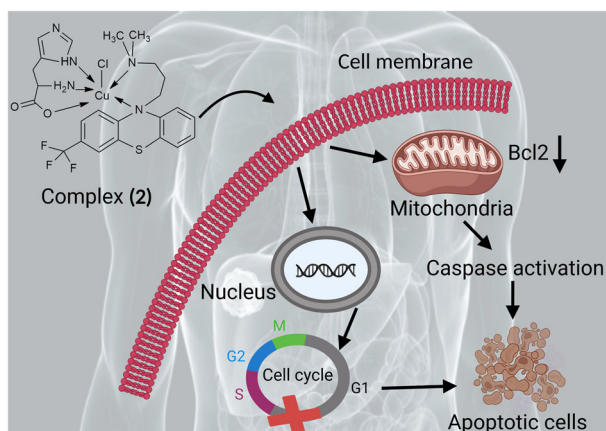
Keywords Cu (II) complexes · Cyclic voltammetry · Biological applications · Gene expression · Protein expression · Molecular modeling

✉ Heba K. A. Elhakim
hebak@sci.cu.edu.eg

1 Biotechnology department, Faculty of Science, Cairo University, Giza 12613, Egypt

2 Inorganic Chemistry Division, Chemistry Department, Faculty of Science, Cairo University, Giza 12613, Egypt

3 Biochemistry Division, Chemistry Department, Faculty of Science, Cairo University, Giza 12613, Egypt

Introduction

Cancer, the most lethal disease, poses a significant challenge in the medical field. Researchers have yet to find appropriate drugs to combat its rapid spread. Consequently, there is an urgent requirement for the development of effective medication to treat cancer [1]. Pharmaceutical research related to anticancer drugs is currently rapidly developing [2]. Even though most of the compounds used in medicine are organic or derived from natural products, the discovery of the anti-tumor properties of Cisplatin led to several studies investigating the potential anticancer effects of other metal compounds [3]. Rosenberg's discovery of Cisplatin in 1965 as a potent anticancer agent and subsequent approval for clinical use have sparked interest in developing successive generations of platinum-based medicines, including carboplatin and oxaliplatin [4, 5]. Although Cisplatin has clinical applications, its significant side effects, low solubility, lack of selectivity, high in vitro toxicity to normal cells, and increased drug resistance limit its use [1, 6].

Since coordination metal complexes are highly useful in cancer chemotherapy, finding new compounds with antitumor activity has become increasingly critical. Anticancer drugs induce intentional cell death, also known as cell apoptosis, by activating intracellular death programs. Additionally, these treatments can also cause accidental cell death, known as cell necrosis, as a result of stress or nutrient deprivation. Cell necrosis initiates with cellular edema, resulting in plasma and organelle membrane rupture and inflammation [7, 8]. One strategy is to study coordination compounds containing essential transition metals as central atoms to find compounds with fewer side effects and a broader spectrum of action than cisplatin [6]. Transition metal complexes have recently been extensively studied for their potential health benefits and biological applications [9].

Cu (II) is essential in biological systems, including normal human metabolism, and is a pharmacological agent found in various enzymes [10, 11]. In addition, synthetic Cu (II) complexes have been reported to have anticancer properties. Numerous Cu (II) complexes have been active both in vitro and in vivo [12, 13]. Depending on the choice of ligand, Cu (II) complexes may exhibit different properties and be used in different ways [14]. In particular, Cu (II) complexes derived from amino acids are highly valuable not only from an inorganic perspective but also from a biological perspective [15]. According to Grosser, amino acids have antioxidant properties [16]. In proteins and enzymes, amino acid residues are bound to metal centers within active sites.

Several studies have demonstrated that phenothiazines exhibit specific cytotoxicity and antiproliferative properties and promote apoptosis in cancer cells at clinically relevant doses without having adverse effects on normal cells [17]. According to several studies, phenothiazines are cytostatic rather than

cytotoxic [18]. They also exhibit antibacterial, antifungal, antiviral, anti-inflammatory, and antiparasite activity [19]. Recent studies have demonstrated that the activity of phenothiazines can be enhanced by complexing them with metal ions [19]. Triflupromazine (TFP) is a member of the phenothiazine family that acts on the central nervous system. It is primarily used to treat schizophrenia and psychosis. TFP's antipsychotic effects are due to dopamine receptor blocking [20]. The cancer risk for patients with schizophrenia is lower (1.93%) than that for patients without schizophrenia (2.97%) [21]. Furthermore, people with certain CNS disorders have been reported to have inverse cancer comorbidities, and pharmacological treatments may be responsible for this phenomenon [22]. Triflupromazine, like other phenothiazine derivatives, exerts anti-calmodulin activity, inhibits kinase C, and inhibits P-glycoprotein transport function, supporting its use as a cancer chemopreventive agent [23].

With the above in mind, in our current study, mixed ligand Cu (II) complexes containing triflupromazine (TFP) as a primary ligand as well as glycine (Gly) and histidine (His) as secondary ligands with the formulas [Cu(TFP)(Gly)Cl]•$2H_2O$ (**1**) as well as [Cu(TFP)(His)Cl]•$2H_2O$ (**2**) were prepared, characterized, and tested to identify several biological activities. Combining Cu (II) with these biologically active ligands can enhance complex activities in cancer treatment, viral treatment, and other biological applications.

Based on our previous finding [24], the observed pharmacological properties of these complexes support continuing the study of their biological applications, such as antiviral activity against three different types of viruses: low-pathogenic Coronavirus 229E, Herpes Simplex type-2 virus (HSV-2), Vesicular Stomatitis Virus (VSV), antiparasite drugs against *Trichinella spiralis* adult worm, anti-inflammatory activities and antitumor properties towards breast cancer cells (MCF-7), liver cancer cells (HepG2), and human skin fibroblast normal cells (HSF). The impacts of complexes on wound healing, the cell cycle, and cell apoptosis are examined.

Gene expression was also studied using RT-PCR technology on pro- and anti-apoptotic genes, in addition to evaluating the level of their corresponding proteins using western blot techniques. A molecular modeling technique was performed to demonstrate the tested complexes' capacity to interact with and inhibit the Bcl2 protein. Cyclic voltammetry experiments were also applied to examine their binding ability to CT-DNA.

Materials and Methods

Cyclic Voltammetry

Electrochemical analyses were performed at room temperature using a 10.00 mL electrolytic cell containing a supporting

electrolyte solution buffer consisting of 5.00 mM Tris-HCl and 50.00 mM NaCl at a pH of 7.10. Before each experiment, the platinum electrode's surface was cleaned in water and freshly polished with 0.05 mm α-Al$_2$O$_3$ paste. After each electrochemical test, the working electrode was cleaned. Without CT-DNA, the voltammogram of 10.00 mL of the complex solution [complex] = 20.00 mM was measured. Similarly, the procedure was performed again for systems with constant concentrations of complexes ([complex] = 20.00 mM) and various concentrations of CT-DNA ([CT-DNA] = 60.00, 80.00, 100.00, and 120.00 μM).

Antiviral Activity

Low-pathogenic Coronavirus 229E, Herpes Simplex type-2 virus (HSV-2), Vesicular Stomatitis Virus (VSV), and Vero E6 cells were provided by Nawah-Scientific, Egypt. An antibiotic solution of 1% was added to the DMEM medium containing 10% fetal bovine serum (FBS); Vero E6 cells were seeded. Gibco-BRL (Grand Island, New York, United states) supplied DMEM, trypsin-EDTA, BSA, and antibiotic solutions. Antiviral and cytotoxic properties were evaluated using the crystal violet method. This was used to demonstrate the inhibitory effects of cytopathic (CPE) complexes [25, 26]. Vero E6 cells were plated with 2.00×10^4 cells per 96-well plate prior to infection. PBS was used to remove the growth media from the cells the next day. For testing the infectivity of 229E, HSV-2, and VSV, the crystal violet technique was applied, which measures cell viability percentages and measures CPE. In mammalian cells, 0.10 mL of diluted viral suspensions of 229E, HSV-2, and VSV with CCID50 (1.00×10^6) of virus stock were used. The recommended dosage was selected after 2 days of infection to induce the required CPEs. Cells were incubated in 0.01 mL of medium that contained the appropriate complex concentration. Antiviral activity was tested on each sample at 10-fold diluted concentrations (0.10–1000.00 μM). Cell controls are un-infected, non-drug-treated cells, and viral controls are virus-infected, non-drug-treated cells. Growth plates were incubated at 37 °C in 5% CO$_2$ for 3 days. The light microscope was applied to investigate cytopathic effects. For fixing and dyeing the thin cell layers, 2% ethanol and 10% formalin were added to a solution of 0.03% crystal violet. They were washed in PBS. Following rinsing and drying, the optical density (OD) was measured at 570/630 nm. Based on Pauwels et al., the formula below is used to determine the percentage of antiviral efficacy in test samples:

$$\text{Antiviral efficacy} = \frac{(\text{mean OD of cell controls} - \text{mean OD of virus controls})}{(\text{OD of test samples} - \text{mean OD of virus controls})} \times 100\%$$

(1)

The 50% inhibitory dosage (IC$_{50}$) of CPE was determined using the GraphPad PRISM software. IC$_{50}$ is the inhibitory concentration required to prevent 50% of viral infections [27]. CC$_{50}$/IC$_{50}$ was calculated to obtain the selectivity index (SI) [28]. This index, often known as a therapeutic index, was used to decide if a drug was worthy of further investigation. Active compounds have a SI ≥ 2, while extremely active compounds have a SI ≥ 10 [29].

Before this essay, we assessed cytotoxicity to see how the complexes affect the viability of Vero 6E cells. At a density of 2.00×10^4, cells were plated in 96-well plates. An additional day later, the cells were exposed to serial dilutions of complexes (0.10–1000.00 μM) for 48 h before being eliminated. PBS was utilized as a washing solution for the cells. The antiviral efficacy assay was performed similarly to that described above.

In Vitro Antitrichinellosis Activity

Adult *Trichinella spiralis* worms were collected from the Theodor Bilharz Research Institute (TBRI). *T. spiralis* (the number of parasites per well ranging from 20.00 to 25.00) was grown on a 24-well plate using RPMI-1640 medium containing 200.00 μg/mL streptomycin and 200.00 μg/mL penicillin with 20% FBS. In this study, four groups were formed: group I: parasites grown only in a medium; group II: parasites grown in a medium containing three concentrations (30.00, 50.00, and 100.00 μg/mL) of complex (**1**) that was dissolved in dimethyl sulfoxide (DMSO); group III: parasites grown in a medium with three concentrations (30.00, 50.00, and 100.00 μg/mL) of complex (**2**) solubilized in DMSO [30]; and group IV: parasites grown in a medium containing 50.00 μg/mL albendazole dissolved in DMSO [31]. For each group, three wells were used, and the plate was incubated for 48 h at 37 °C with 5% CO$_2$; then, the whole adult worm groups were gathered for examination under the microscope.

Scanning electron microscopy (SEM)

Abou Rayia et al. described the procedure for processing adult worms after 48 h [32]. The worms were incubated overnight at 4 °C in a fixation solution containing 2.5% glutaraldehyde buffered with 0.10 M sodium cacodylate at pH 7.20. After 5 min of washing in 0.10 M sodium cacodylate buffer at pH 7.20, specimens were post-fixed in 2% osmium tetroxide for 1 h. Ethyl alcohol was used in increasing concentrations to dry the samples before placing them on carbon-coated adhesive material. The samples were then subsequently examined by a JEOL JSM-6510LV scanning electron microscope (SEM), Japan [33].

Red Blood Cell Membrane Stabilization Activity (Anti-inflammatory Studies)

A UV–vis spectrophotometer (BMG LABTECH, Offenburg, Germany) was used in measuring the anti-inflammatory effects of complexes (1) and (2) three times for each complex.

Preparation of erythrocyte suspension

According to Anosike et al., an erythrocyte suspension was prepared [34]. Healthy fresh blood samples (3.00 mL) were drawn in tubes with heparin and centrifuged at 3000 rpm for 10 min (the blood sample used in the current study was acquired from a volunteer). A saline solution was added to the red blood pellets in an amount equivalent to the supernatant. Dissolved red blood pellets were determined and prepared in an isotonic buffer (10.00 mM sodium phosphate buffer, pH 7.30). In 1 l of distilled water, the buffer solution contained 0.20 g of NaH_2PO_4, 1.15 g of Na_2HPO_4, and 9.00 g of NaCl. The sample was composed of blood cells (resuspended supernatant).

Hypotonicity induced hemolysis

This test used pure distilled water (hypotonic solution) to dissolve the samples. Several concentrations of samples (100.00, 200.00, 400.00, 600.00, 800.00, and 1000.00 μg/mL) were added to a hypotonic solution (5.00 mL) and placed in duplicate pairs of centrifuge tubes. In addition, duplicate pairs of centrifuge tubes (per dosage) were filled with an isotonic solution (5.00 mL) containing different concentrations of samples (100.00–1000.00 μg/mL). Each control tube contained 5.00 mL of 200.00 μg/mL of diclofenac and 5.00 mL of vehicle (distilled water). In each tube, 0.10 mL of erythrocyte suspension was added, which was thoroughly mixed. The samples were centrifuged at 1300 g for 3 min after incubation for 1 h at 37 °C. At 540 nm, the absorbance (OD) of the resultant supernatant's hemoglobin concentration was determined. The hemolysis percentage was calculated by assuming hemolysis occurred at 100% in distilled water. The following Equation determines the mixture's percent hemolysis inhibition [34] (2):

$$\%\text{Hemolysis inhibition} = 1 - \left(\frac{OD2 - OD1}{OD3 - OD1}\right) \times 100 \quad (2)$$

Assuming that OD1 is the tested complex's absorbance in an isotonic solution

OD2 is the tested complex's absorbance in a hypotonic solution.

OD3 is the absorbance of the reference drug in a hypotonic solution.

The blood control drug used was diclofenac, which represents 100% lysis.

Cell Cultures

Nawah Scientific Inc., (Mokatam, Cairo, Egypt), provided the cell lines (MCF-7) breast cancer cell, (HepG2) liver cancer cell, and (HSF) human skin fibroblast. At 37 °C, cells were cultured in DMEM in an atmosphere of 5% (v/v) CO_2, supplied with 100.00 units/mL penicillin, 100.00 mg/mL streptomycin, and 10% heat-inactivated fetal bovine serum.

Anticancer activity (cytotoxicity assay)

The sulphorhodamine-B (SRB) method was applied to study the cytotoxicity potential of the synthesized complexes. In a 96-well plate, HSF, MCF-7, and HepG2 cells were grown for 24 h prior to exposure to the tested samples to promote cell attachment. Various concentrations of the complexes under test (100.00, 10.00, 1.00, 0.10, and 0.01 μg/mL) were applied to the cell monolayer. Triplicate wells were used for each dose. In a 5% CO_2 atmosphere, cells were incubated at 37 °C with the tested samples for 72 h. Following 72 h, the cells were fixed, rinsed, and dyed with sulphorhodamine-B (SRB). Acetic acid was utilized to remove the excess stain, and Tris-EDTA buffer was used to recover the attached stain. Finally, a microplate reader (BMGLABTECH®FLUOstar Omega, Germany) was utilized to measure absorbance at 540 nm. To determine the IC_{50} values, a graph plotting the percentage of cell inhibition against the concentration was used [35].

Cellular drug uptake

MCF-7 and HepG2 cells were seeded in 6-well plates. Upon reaching 80% confluence, the IC_{50} values of complex (2) on MCF-7 and HepG2 were 40.25 and 35.36 μg/mL, respectively. Ice-cold PBS was applied to thoroughly rinse the cells more than two times after 72 h of incubation with complex (2). A centrifuge was used for 10 min at 1000 g to resuspend the cells in 1.00 mL of PBS. 100.00 μL was measured to determine cell density. The rest of the cells were dissolved in 0.50 mL of lysis buffer. They were vortexed for 5 min to dissolve. In the HPLC system, 50.00 μL of the sample was injected [36].

Wound healing assay

For the scratch wound experiment, cancer cells (MCF-7) and (HepG2) were plated onto a coated 12-well plate at a density of 2.00×10^5 in 5% CO_2 and 5% FBS-DMEM for

24 h at 37 °C. On the following day, the confluent monolayer was scratched horizontally. After thoroughly rinsing the plate in PBS, the control wells were refilled with freshly formulated medium. The tested Cu (II) complexes were treated with fresh medium. An inverted microscope was used to capture images at specific intervals. At each time point, the plate was incubated with 5% CO_2 at 37 °C. The captured images were examined using MII ImageView software version 3.7 [37].

Cell cycle analysis

The synthesized Cu (II) complexes are treated for the specified period, and then cells (10^5 cells) are isolated by trypsinization and rinsed two times using ice-cold PBS (pH 7.30). Fixation is achieved by resuspending the cells for 1 h at 4 °C in 2.00 mL of 60% ethanol. Upon rinsing two times in PBS (pH 7.30), the cells are suspended in 1.00 mL of PBS supplemented with RNAase A (50.00 µg/mL) in addition to propidium iodide (PI) (10.00 µg/mL). An ACEA Novocyte^{TM} flow cytometer (ACEA Biosciences Inc., San Diego, California, United States) ACEA Biosciences, Inc., San Diego, California, United States) is used to determine DNA content after incubating the cells in the dark for 20 min at 37 °C. There are 12,000 events recorded for each complex. This test utilizes ACEA NovoExpress^{TM} software (ACEA Biosciences Inc., San Diego, California, United States) to determine cell cycle progression [38].

Cell apoptosis analysis

Annexin V-FITC apoptosis detection kits (Abcam Inc., Cambridge Science Park, Cambridge, UK) and two fluorescent flow cytometry channels were used to examine apoptotic cell populations. After exposure to Cu (II) complexes (**1**) and (**2**) for 72 h, cells (10^5 cells) are trypsinized and rinsed twice using PBS (pH 7.40). Afterward, cells are exposed to 0.50 mL of Annexin V-FITC/PI reagent at room temperature for 30 min without light. ACEA Novocyte^{TM} flow cytometers (ACEA Biosciences Inc., San Diego, California, United States) were used to assess stained cells for FITC and PI fluorescence (λex/em 488/530 nm and 535/617 nm, respectively). The total number of events examined for each complex is 12,000; PI and/or FITC-positive cells are determined using the software ACEA NovoExpress^{TM} (ACEA Biosciences Inc., San Diego, California, United States) [39].

Gene expression

MCF-7, HepG2, and HSF cells were exposed to Cu (II) complexes (**1**) and (**2**), in which the SRB assay identified the cytotoxicity potentials. Cells were exposed to complex (**1**) and complex (**2**) and incubated for different time intervals: 24, 48, and 72 h. RNA was then isolated by the Purelink® RNA Mini Kit (Ambion®, Inc., US). RNA samples were tested for concentration and purity with a Nano-Drop spectrophotometer. The RevertAid First Strand cDNA Synthesis Kit from Thermo Fisher Scientific, United States, was applied to convert 1.00 mg of total RNA into cDNA. p53, BAX, Caspase 3, and Bcl2 expression levels were assessed. β-actin was used as a housekeeping gene. (p53 primer: F-5′AGCGAGCACTGCCCAACA3′, R-5′CACGCCCACGGATCTGAA3′; BAX primer: F-5′ATGCGTCCACCAAGAAGC3′, R-5′ACGGCGGCAATCATCCTC3′; Caspase 3 primer: F-5′TTCATTATTCAGGCCTGCCGAGG3', R-5′TTCTGACAGGCCATGTCATCCTCA3′; Bcl2 primer: F-5′GTGTGGAGAGCGTCAACC3′, R-5′CTTCAGAGACAGCCAGGAG3′ and β-actin primer: F-5′TCTGGCACCACACCTTCTACAATG3′, R-5′AGCACAGCCTGGATAGCAACG3′). Real-time PCR was conducted on cDNA utilizing GeneSure^{TM}SYBR Green/ROX qPCR Master Mix (2x) (Genetix Biotech Asia Pvt. Ltd.). The comparative threshold (Ct) approach was utilized to assess the quantitative RT-PCR data and compare the fold inductions of the treated and untreated samples [40].

Western blot analysis

Western blotting is a technique used to find specific proteins in a sample. This technique is known as protein immunoblotting since it uses antibodies to detect antigens. Based on the location and intensity of the bands that appear, it is possible to identify the exact expression pattern of the target proteins within the cells [41]. A density of 5.00×10^6 cells was plated in each well. The respective IC_{50} concentrations of both Cu (II) complexes were applied for 72 h to MCF-7 and HepG2 cells. After trypsinization, the cells were gathered and rinsed two times using PBS. A 1% cocktail (Sigma-Aldrich, United States) of RIPA buffer (Beyotime Biotech., Nantong, China) lysed the cells. The protein content of the supernatant was measured using the Flash Multimode Varioskan instrument (Thermo Fischer Scientific Inc.) and Bradford reagent (Bio-Rad, USA) after centrifugation at 12,000 rpm for 10 min at 4 °C. Separation of protein (40 µg per lane) was performed on 12% SDS-PAGE and moved to a Hybond™ nylon membrane (GE Healthcare) using the TE62 Standard Transfer Tank with Cooling Chamber (Hoefer Inc., Germany). A tris-buffered saline solution containing 0.10% Tween 20 (TBST) with 5% blocking powder (Santa Cruz) was used to block the membrane for 2 h at room temperature. Following a TBST rinse for 5 min, the primary antibody (Abcam, Cambridge, UK) was applied and overnight incubated. The membrane was then exposed for 1 h at room temperature to the corresponding horseradish peroxidase
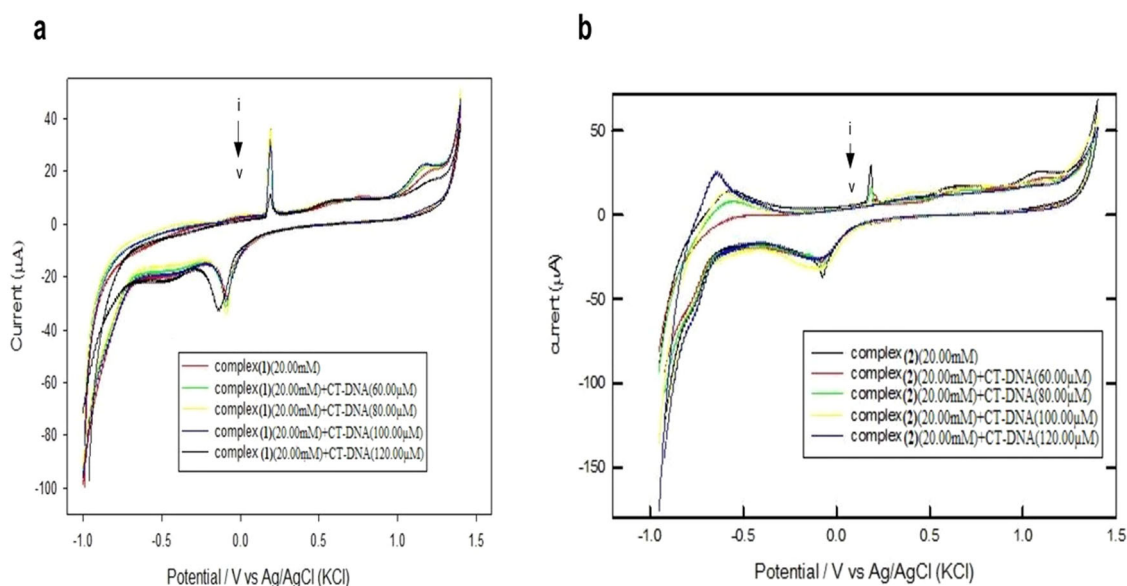
Fig. 1 a, **b** Cyclic voltammograms of Cu (II) complexes (**1**) and (**2**), respectively, without and with CT-DNA in Tris-HCl buffer. [Complex] = 20.00 mM (i); from ii to v, [CT-DNA] = 60.00, 80.00, 100.00, and 120.00 μM, respectively

(HRP)-labeled secondary antibody (Abcam, Cambridge, UK). A gel documentation system (Geldoc-it, UVP, England) was used and TotalLab analysis software (Version 1.0.1), www.totallab.com, was applied for data analysis.

Molecular Docking Study

AutoDock software tool (ADT) version 4.2.6 was utilized to perform molecular docking analyses [42]. Using the Protein Data Bank (PDB), B-cell lymphoma 2 (Bcl2) was downloaded (PDB ID: 4IEH). Using ADT, water was removed, and polar hydrogen atoms were introduced. Every atom was charged with a Kollman charge and merged with a non-polar hydrogen atom. The structure was saved as PDBQT. Using ChemSketch, the synthesized complexes were drawn and saved. Minimized complexes were anchored to receptor-active sites. The grid box displayed only active receptor sites based on specific amino acid residues. AutoDock 4.2.6 software settings are default-selected. CHIMERA was used to evaluate docking results [43]. It can visualize receptor-ligand docking and estimate hydrogen bonding feasibility between receptors and ligands. Low energy indicates proper binding between ligand and receptor.

Statistical Analysis

The data was evaluated for normal distribution and then analyzed using one-way and two-way analysis of variance (ANOVA) in GraphPad PRISM software (*GraphPad Software, San Diego, USA*), version 8. A significance threshold of *P < 0.05 was deemed acceptable for statistical significance.

Result and Discussion

Cyclic Voltammetry

A cyclic voltammogram of the tested complexes is presented in Fig. 1a, b, without and with various DNA concentration levels. In the cyclic voltammogram of complex (**1**) (Fig. 2a), the cathodic peak potential (E_{pc}) is −0.0755 V, and the anodic peak potential (E_{pa}) is 0.1996 V. The separation of cathodic and anodic peak potentials (ΔE_p) is −0.275 V. I_{pc}/I_{pa} is the ratio between cathodic and anodic peak currents, which is −0.883, suggesting a quasi-reversible redox reaction. Without CT-DNA, the formal potential ($E_{1/2}$), the average of E_{pc} and E_{pa}, is 0.062 V. As CT-DNA is incrementally added to the complex (**1**), it leads to a shift in $E_{1/2}$ of 0.027 V and a reduction in ΔE_p of about −0.332 V. The I_{pc}/I_{pa} ratio is −1.90 for cathodic to anodic peak currents. The cyclic voltammograms of complex (**2**), $E_{1/2}$, ΔE_p, and I_{pc}/I_{pa} values are 0.0523 V, −0.2611 V, and −1.253, respectively, without CT-DNA. Complex (**2**) shows a change in $E_{1/2}$ (−0.1313 V), ΔE_p (−1.055 V), and the cathodic to anodic current peak I_{pc}/I_{pa} ratio is −2.37 when CT-DNA is added under the same conditions (Fig. 2b). A variation in formal potential indicates that the drug interacts with DNA. Previous studies have indicated that positive shifts (anodic shifts) in formal potential occur when cationic drugs are intercalated into DNA's double helical structure [44]. In contrast, negative shifts are observed when cationic drugs interact electrostatically with DNA's anionic phosphate backbone [45, 46]. Consequently, the cathodic shift in peak potential observed in the
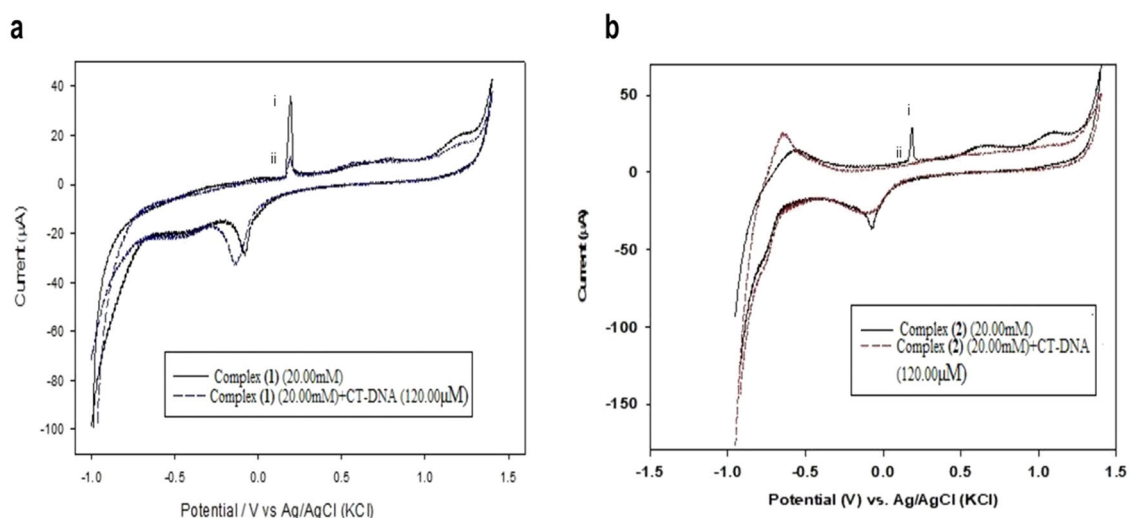
Fig. 2 a, b Cyclic voltammograms of Cu (II) complexes (1) and (2), respectively, at a scan rate of 200 mV s^{-1} in a Tris-HCl buffer (i) without CT-DNA and (ii) with CT-DNA

Table 1 Antiviral activity of the tested complexes (1) and (2) in terms of CC$_{50}$, IC$_{50}$, and SI against 229E, HSV-2, and VSV

Cu (II) Complexes	Viruses								
	229E			HSV-2			VSV		
	CC$_{50}$ (µM)	IC$_{50}$ (µM)	SI	CC$_{50}$ (µM)	IC$_{50}$ (µM)	SI	CC$_{50}$ (µM)	IC$_{50}$ (µM)	SI
Complex (1)	46.71	2.35	19.90	34.25	4.58	7.47	18.40	167.67	0.11
Complex (2)	81.86	1.51	54.40	39.47	4.24	9.30	40.50	9.39	4.30

tested complexes in the existence of polyanionic DNA supports our prior observation that they react electrostatically [24].

Antiviral activity

The antiviral effects of prepared complexes on low-pathogenic Coronavirus 229E, Herpes Simplex type-2 virus (HSV-2), and Vesicular Stomatitis Virus (VSV) were evaluated by cytopathic effect (CPE) using a crystal violet assay. The cytotoxicity of the tested complexes on Vero E6 cells of the viruses mentioned above was evaluated before antiviral activity testing. An antivirus agent should kill the virus without harming Vero 6E cells. Regression analysis represented cytotoxicity as the CC$_{50}$, the concentration of drugs required to impede cell proliferation up to 50%. When the cells were exposed to Cu (II) complexes (1) and (2) at various concentrations of 0.10–1000.00 µM for 48 h, complex (2) showed low cytotoxicity in contrast to complex (1), which indicates that complex (2) did not greatly affect the growth of Vero 6E cells other than complex (1) (Table 1 and Fig. 3a).

We performed a CPE inhibition test after identifying the cytotoxicity of Cu (II) complexes to evaluate the antiviral properties of the prepared complexes and to calculate the IC$_{50}$ against 229E, HSV-2, and VSV for complexes (1) and (2). A

crystal violet assay determined the virus's 229E, HSV-2, and VSV titers. Diluted virus concentrations, equivalent to 50% of the cell culture inhibitory dose, were used for seeding viruses throughout the experiments. Table 1 and Fig. 3b show the prepared complexes' inhibitory effects on CPE. The prepared Cu (II) complexes exhibited strong antiviral efficacy against 229E. Both complexes (1) and (2) inhibited viral CPE by 50% at 2.35 and 1.51 µM, respectively. Complex (2) exhibited more potent anti-low pathogenic human Coronavirus (229E) activity than complex (1), so the selective index (SI) of the tested complexes (1) and (2) is 19.90 and 54.40, respectively. For Herpes Simplex type-2 virus (HSV-2), both complexes (1) and (2) showed modest antiviral activity, with IC$_{50}$s of 4.58 µM and 4.24 µM, respectively. Based on the IC$_{50}$ values, complex (2) has higher SI values than complex (1) (9.30 and 7.47, respectively). This demonstrates that complex (2) has effective anti-herpetic efficacy against complex (1). For Vesicular Stomatitis Virus (VSV), complex (1) displayed no antiviral activity with an IC$_{50}$ value of 167.67 µM. In contrast, complex (2) indicated low antiviral activity with an IC$_{50}$ value of 9.39 µM. As a result, both Cu (II) complexes (1) and (2) had SI values of 0.11 and 4.30 against VSV, respectively.

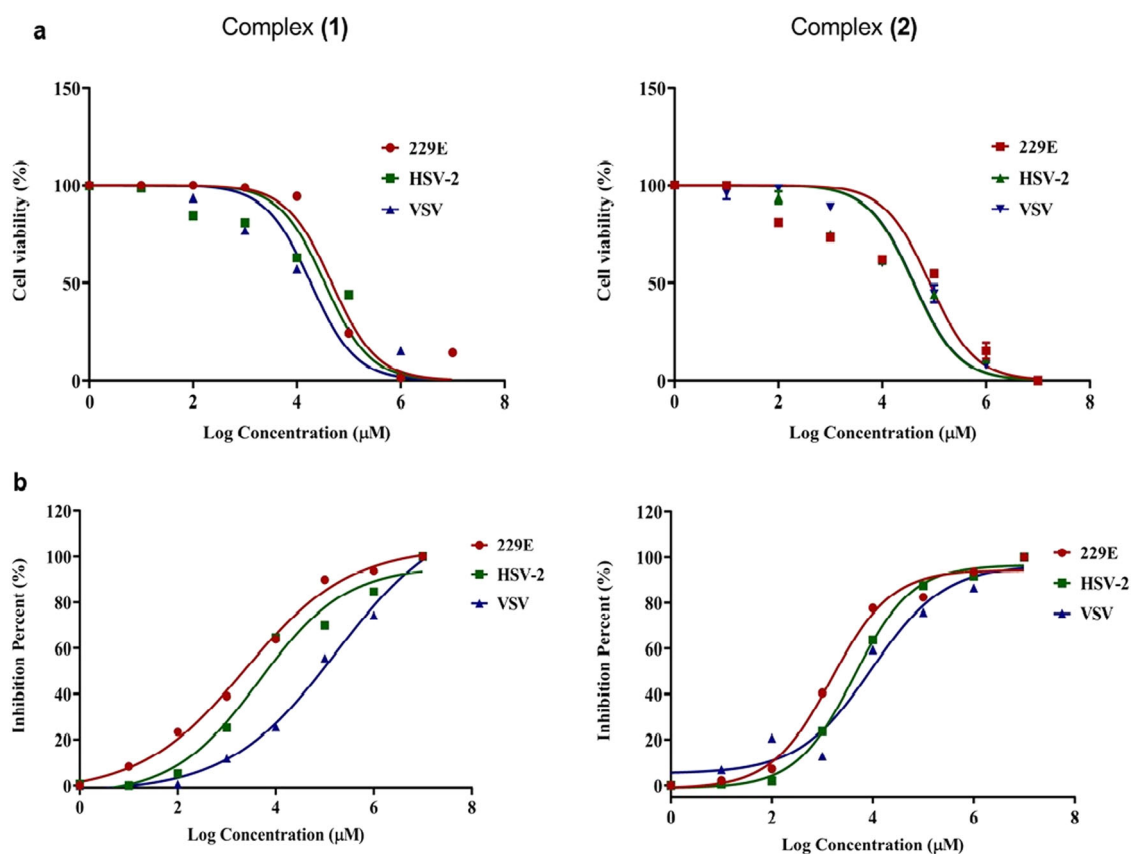Virus infections are still a major public health concern around the world. Unfortunately, several pathogenic viruses

Fig. 3 Antiviral activities of Cu (II) complexes (**1**) and (**2**) against 229E, HSV-2, and VSV (**a**) cytotoxicity of the tested complexes to Vero E6 cells (**b**) displayed CPE inhibition using the crystal violet assay of the tested complexes on the viruses mentioned above. Each data point represents the average of three independent experiments

still lack effective medications. However, proteins from various species or virus genotypes do not necessarily share structural similarities. In addition, viruses can mutate during replication, so antiviral drugs that target a specific viral protein are not always effective against another virus [47]. First and foremost, we need more countermeasures for viral invasion to provide an immediate treatment response against the virus. As a result, repurposing licensed drugs provides various advantages, including proven safety/tolerance profiles, availability, lower cost, and clinician familiarity with working with these drugs [48]. From the presented findings, complex (**2**) has a stronger antiviral effect than complex (**1**). This may be due to the imidazole ring in histidine, which increases cellular absorption. In addition, the intracellular distribution of the complex into a cell virus leads to cell destruction [49].

In Vitro Antitrichinellosis Activity

Trichinella spiralis adult worms were incubated with three concentrations of the tested complexes for 48 h. Throughout the experiment, the control worms were alive and actively moving under the microscope. At all concentrations tested, the synthesized Cu (II) complexes affected the morphology

of worms and decreased their motor activity. After 2 days, 100% of *T. spiralis* adult worms were killed with complex (**2**) at 100.00 µg/mL. Complex (**2**) was generally more active than complex (**1**). Two days after treatment with complex (**1**), 34% of adult worms were destroyed, whereas, after treatment with complex (**2**), 44% of adult worms were killed at 30.00 µg/mL. Both complexes (**1**) and (**2**) destroyed 45% and 65% of worms after 48 h at a concentration of 50.00 µg/mL, respectively. At a concentration of 100.00 µg/mL, complex (**2**) eradicated 100% of the worms, whereas complex (**1**) destroyed 78% after 48 h. Albendazole was more active on *T. spiralis* worms than the tested complexes. Albendazole, at 50.00 µg/mL, eradicated 100% of adult worms after 36 and 48 h. It is noteworthy that complex (**2**) had a lower LD_{50} than complex (**1**); after two days, the LD_{50} for complex (**2**) was 37.04 µg/mL, and for complex (**1**), it was 40.74 µg/mL (Table 2).

Scanning electron microscopy

Figure 4a, b Scanning electron microscope images of the control group of *Trichinella spiralis* adult worms. (A) the adult worm has the normal whole worm shape,

Table 2 LD_{50} of the tested complexes after 24, 36, and 48 h

Cu (II) complexes	Time (h)	LD_{50} (µg/mL)
Complex (1)	24 h	111.55
	36 h	72.04
	48 h	40.74
Complex (2)	24 h	98.38
	36 h	51.04
	48 h	37.04

demonstrating its typical appearance when removed from its nurse cell, anus (a), and mouth (m). (B) illustrates a cuticle with normal structure and creases (arrow). Figure 4c, d: *T. spiralis* adult worms treated with albendazole (C) adult worms have severe destruction and abnormal shapes: anus (a) and mouth (m). (D) shows numerous fissures in the cuticle with missing annulations and irregular creases (arrow). Figure 4e, f, g: A *T. spiralis* adult worm treated with complex (1) displayed marked signs of starting destruction. (E) illustrates an adult worm losing its normal worm shape and full contraction (red arrow) after the mouth region. (F) shows a shrined cuticle (white arrow) and loss of creases (*). (G) depicts swelling (arrowhead) after the anus region. Figure 4h, i, j: Scanning electron microscope image of a *T. spiralis* adult worm treated with the synthesized complex (2). The worm was fully destroyed (H), losing its entire form and rupturing in the middle. (I) shows a ruptured cuticle (white arrow) and complete loss of the cuticle's creases, ridges, and annulations. (J) shows swelling (arrowhead) and multiple blebs (#).

Trichinellosis medical treatment is controversial. However, albendazole can cause severe systemic effects, including epilepsy, encephalitis, and even death [50, 51]. Based on these findings, it is imperative to develop an innovative, safe, and potent therapy that successfully eliminates *Trichinella spp.* infections. In this experiment, the antiparasitic efficacy of the tested complexes against *Trichinella spp.* was evaluated in vitro. The cuticle, hypodermis, and somatic musculature comprise the *Trichinella* body wall. Cuticle integrity affects parasite formation, feeding, and defense. Osmoregulation also depends on the cuticle [52]. Adult worms suffered significant damage in our investigation, including cuticle swelling, regions with vesicles, blebs, and missing annulations. These were among the groups exposed to synthesized complexes and albendazole. Therefore, all of these findings indicate effective antiparasitic action [53]. This could make it easier to understand how Cu (II) complexes (1) and (2) work. Complex (2) is more active than complex (1); this may be related to histidine, which contains an imidazole ring that can disrupt cell division and energy pathways and interfere with similar vital processes, resulting in parasite death [54].

Red Blood Cell Membrane Stabilization Assay (Anti-Inflammatory Activity)

Leukocytes release lysosomal enzymes during inflammation to prevent tissue damage and further inflammation [55]. Through lipid peroxidation, free radicals damage cell membranes. It is essential to use anti-inflammatory agents to prevent inflammation and protect the cell membrane from harmful substances. As shown in Fig. S1, the tested Cu (II) complexes (1) and (2) helped maintain erythrocytes' membrane integrity. The results revealed that the studied Cu (II) complexes had powerful actions. This shows that they strongly affect human erythrocytes, protecting them from hypotonic lysis. The concentration ranges demonstrated that the tested Cu (II) complexes had dose-dependent membrane stabilization. Complex (1) exhibited a minimum membrane stability of 64.20% at 100.00 µg/mL and a maximum activity of 95.50% at 1000.00 µg/mL, whereas complex (2) displayed a minimum membrane stability of 69.10% at 100.00 µg/mL and a maximum efficacy of 99.20% at 1000.00 µg/mL.

Figure S1 illustrates that complex (2) provides more effective protection against induced lysis than complex (1). Therefore, the imidazole ring and coordination of histidine increased membrane stability.

The results of this experiment indicated that the prepared Cu (II) complexes effectively prevented erythrocyte membrane lysis. The observed activity may be caused by the coordination of substituents in the complexes and their ability to bind to ions and molecules on the erythrocyte membrane [56].

Figure S1. Effect of the tested Cu (II) complexes on HRBCs hemolysis inhibition. Results are presented as mean ± SD. Statistical significance levels between the treated groups and control groups consisted of ns = non-significant, $*P < 0.05$, $**P < 0.01$, $***P < 0.001$, and $****P < 0.0001$.

In Vitro Cytotoxicity Assay

There are multiple complications associated with cancer at the molecular and cellular levels, making it a complex disease. The use of synthesized metal complexes as anticancer agents has proven successful due to their high selectivity for malignant cells. In addition, they inhibit tumor metastasis [57]. The tested complexes were examined for cytotoxicity to three cell lines: HSF, MCF-7, and HepG2. The activities of the tested complexes were determined using the SRB assay, which measures cell viability. The results are presented regarding IC_{50}s, as presented in Table 3 and Fig. 5. The SRB assay demonstrated that complexes (1) and (2) were effective on both cancer cells. However, they showed less activity
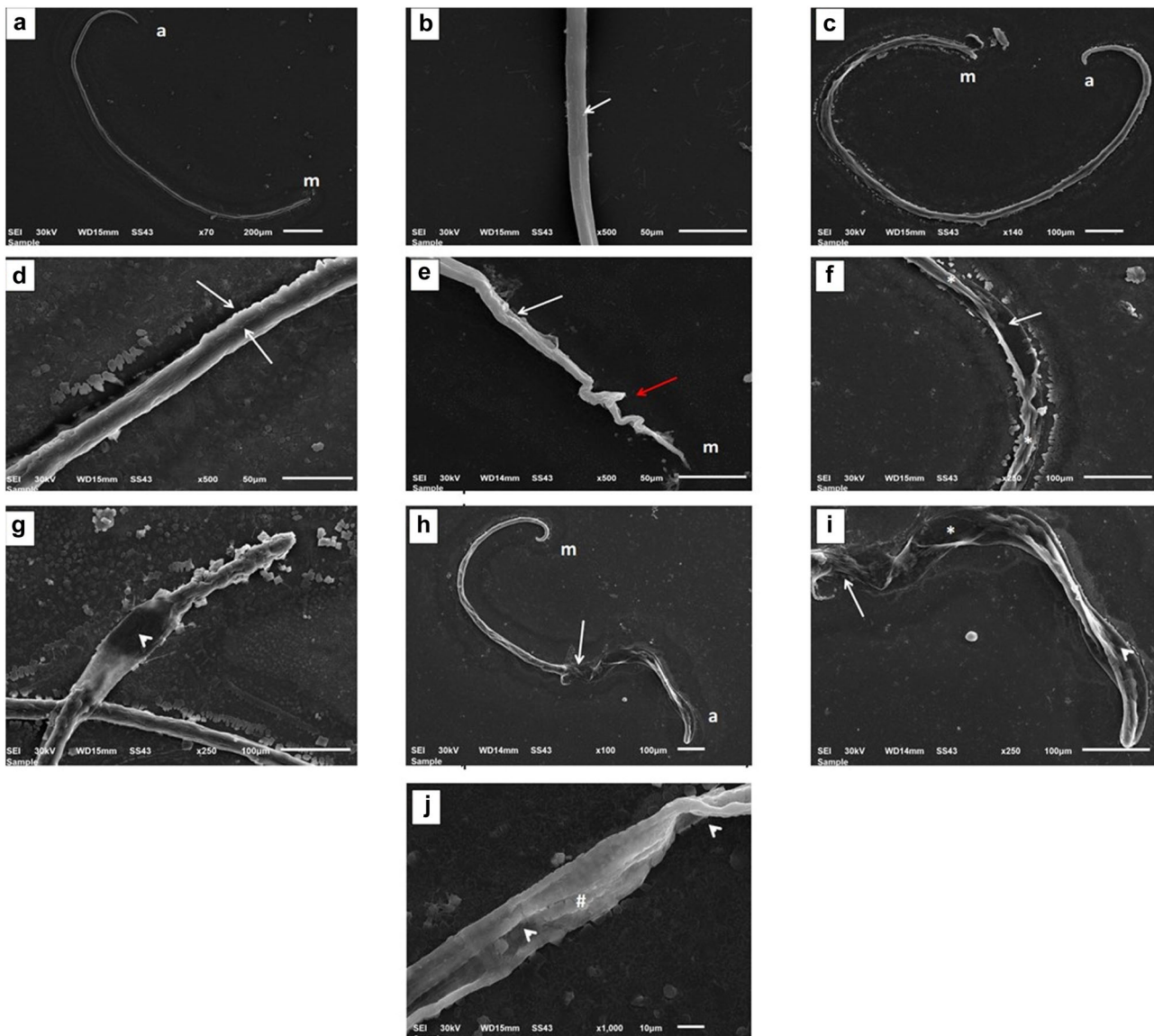
Fig. 4 SEM results of *T. spiralis* adults: **a**, **b** normal adult worm; (**c** and **d**) albendazole-treated group, exhibiting significant destruction of numerous fissures in the cuticle with missing annulations and irregular creases (arrow); **e**, **f**, and **g** complex (**1**) treated group, displaying losing the whole normal worm shape, full contraction (red arrow), shrined cuticle (white arrow), losing of creases (*), and swellings (arrowhead) after anus region; **h**, **i**, and **j** complex (**2**) treated group, presenting complete losing of the normal worm shape, rupturing cuticle (white arrow), total failure of creases, ridges, annulations of the cuticle, swellings (arrowhead), and multiple blebs (#)

against the normal cell (HSF), especially complex (**2**). This confirms the synthesized Cu (II) complexes' cytotoxic effects on cancer cells. Based on the complexes examined here, complex (**2**) is more cytotoxic than complex (**1**) on both cancer cell lines.

Furthermore, this study indicates that the tested Cu (II) complexes, particularly complex (**2**), are more toxic to liver cancer cells than to breast cancer cells. The higher cytotoxicity of complex (**2**) is consistent with its increased ability to bind DNA, which was confirmed in our previous work [24], and this confirms the concept that binding complexes to DNA results in cell death [2].

Table 3 The cytotoxic properties of the tested complexes

Cu (II) complexes	IC_{50} µg/mL		
	HSF	MCF-7	HepG2
Complex (**1**)	112.02	51.21	44.92
Complex (**2**)	182.84	40.25	35.36

Cellular Drug Uptake

Since complex (**2**) exhibited higher anticancer activity in MCF-7 and HepG2 than complex (**1**), it was chosen to
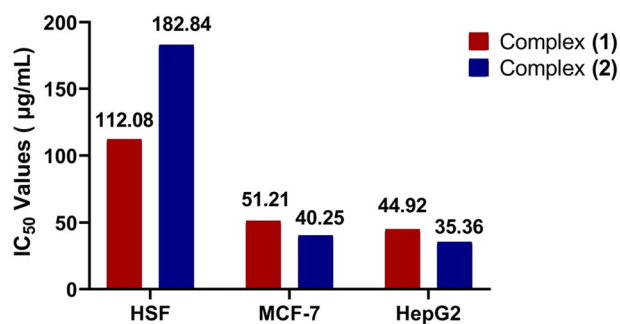
Fig. 5 IC_{50} values derived from anticancer studies of the tested Cu (II) complexes are compared with HSF, MCF-7, and HepG2

examine the relationship between cell uptake, in vitro cytotoxicity, and the selectivity of complex (**2**) towards cancer cells. To understand the intake of complex (**2**) in both cancer cell lines, a cellular intake experiment was performed. Figure S2 shows that the treatment of HepG2 cells with complex (**2**) (35.36 µg/mL) for 72 h showed an increase in the cellular complex (**2**) concentration (66.00 µg/mL) compared with the treatment of MCF-7 with complex (**2**) (40.25 µg/mL) for 72 h that showed a low concentration of cellular intake (55.69 µg/mL), suggesting that HepG2 has a higher sensitivity and selectivity to complex (**2**) than MCF-7. The results of this assay agree with those of the in vitro cytotoxicity assay described above.

Figure S2. Complex (**2**) was used in the treatment of MCF-7 and HepG2 cells (40.25 µg/mL) and (35.36 µg/mL) for 72 h, respectively. There was a highly significant difference between the complex (**2**) uptake by HepG2 and MCF-7 at ****$P < 0.0001$.

Wound Healing Assay

Cell migration plays a crucial role in tissue growth and preservation [58]. The migration of cells plays a vital part in embryonic growth, immune response development, wound healing, and many other biological processes [59]. Several diseases, particularly cancer, are affected by this process, which contributes to invasion and metastasis [60]. The effects of the synthesized complexes on the migration of cancer cells in MCF-7 and HepG2 have been tested using wound healing assays. Figure 6a, c show that the untreated control MCF-7 and HepG2 cells migrate rapidly in a time-dependent manner as a result of their metastatic ability. In contrast, the cells treated with the synthesized complexes do not migrate so quickly. Cu (II) complexes (**1**) as well as (**2**) did not change the wound area in cells incubated with them (Fig. 6b, d, respectively), thus demonstrating their anti-proliferative properties.

Changes in DNA structure and function cause cancer. DNA is one of the most significant targets for cancer therapeutic agents [61]. Therefore, the identification and

characterization of small molecule interactions with DNA has become a focal point of scientific research. The results presented suggest that complex (**2**) exhibits significantly stronger anti-proliferative and anti-invasive characteristics than complex (**1**). This is attributed to the presence of an imidazole ring in histidine, which has distinctly proton-accepting and donating properties [62]. Consequently, imidazole is capable of easily targeting and interacting with DNA both covalently and non-covalently (electrostatically, intercalationally, or via groove binding); this inhibits cell division and cancer cells' migration and invasion capabilities [63].

Cell Cycle Analysis

Anticancer drugs inhibit cancer cell proliferation by arresting the cell cycle, causing apoptosis, or combining these two mechanisms [64]. Flow cytometry was used to determine whether the antiproliferative activities of the tested complexes were triggered by cell cycle arrest. Propidium iodide (PI) staining assessed the cell cycle phase ratio. Figure 7. shows that treatment with complexes (**1**) and (**2**) increased the percentage of cells in the G1 phase and reduced the percentage in the S and G2 phases. This is compared to control cells. In both cancer cells, complex (**2**) showed a greater effect than complex (**1**). Both complexes affected HepG2 (Fig. 7b) better than MCF-7 (Fig. 7a). During the G1 phase, the tested complexes inhibited the proliferation of MCF-7 and HepG2 cells.

Cell Apoptosis Analysis

To further study if the effective antiproliferative effect of the tested complexes was related to the activation of cancer cell apoptosis, we conducted flow cytometry analysis on MCF-7 and HepG2 cells and assessed the percentage of apoptotic cells. Both cancer cells were incubated with IC_{50} concentrations of the tested complexes for 72 h, and then the cells' apoptosis rate was determined using FCM. Compared to control cells, cancer cell lines exhibit remarkably high levels of apoptosis in response to both Cu (II) complexes, as shown in Fig. 8. In breast cancer (MCF-7) as well as liver cancer (HepG2) cells, complex (**1**) induced 5.56 and 6.22% apoptosis, while complex (**2**) caused 7.33 and 8.77% apoptosis, respectively. These results indicate that both complexes could induce apoptosis in cancer cells. However, complex (**2**) exhibits higher apoptotic ability than complex (**1**).

Evaluation of Selected Apoptotic and Anti-apoptotic Gene Expression in MCF-7, HepG2, and HSF Cells

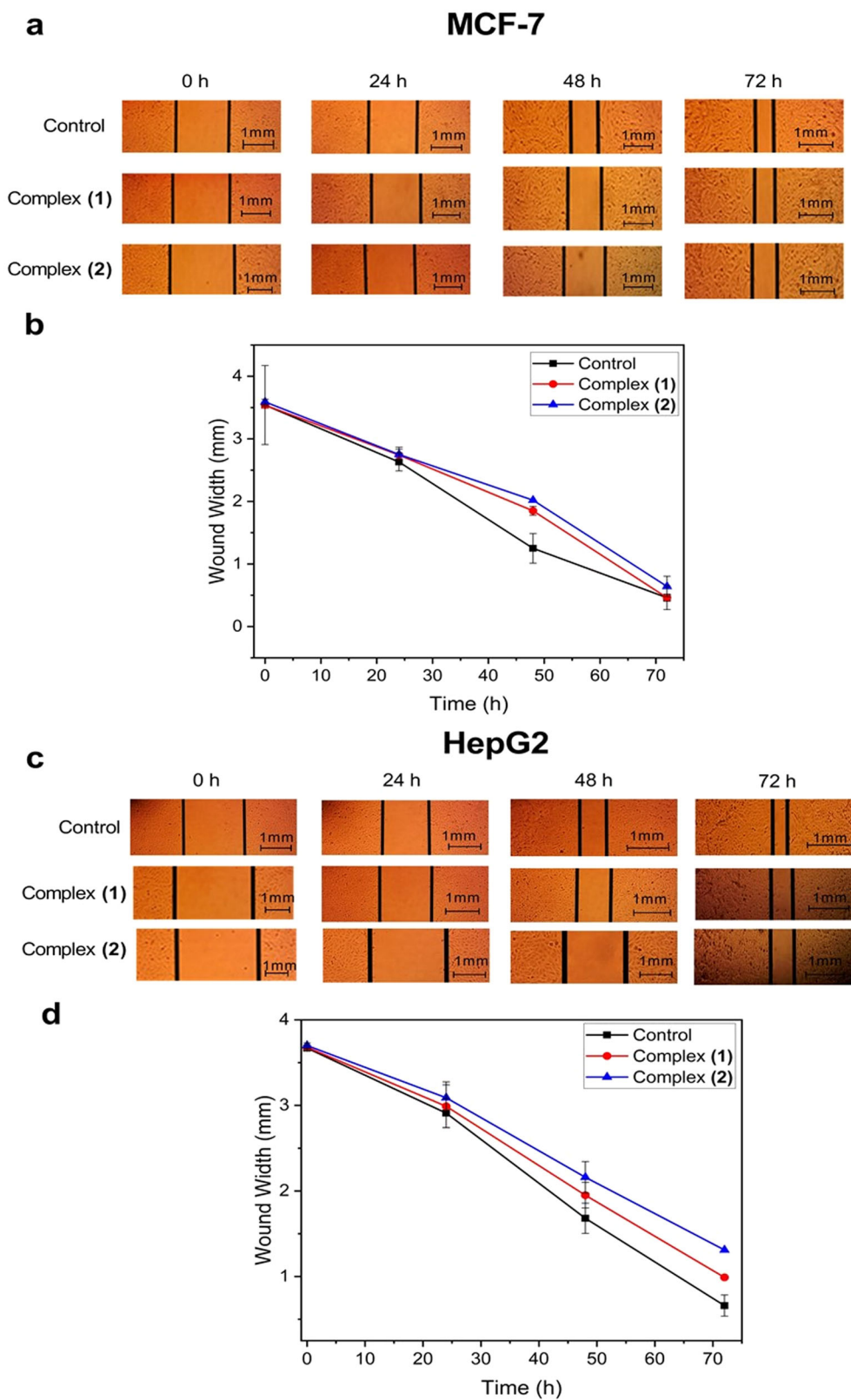Apoptosis (programmed death of cells) inhibition is critical in tumor formation because it permits abnormal cell

Fig. 6 In vitro wound healing study in cancer cell lines. **a**, **c** Untreated control cells of MCF-7 and HepG2 migrate rapidly toward the wound area with time, respectively. In contrast, cells treated with the tested complexes, particularly complex (**2**), cannot migrate rapidly compared to untreated controls. Scale bar: 1 mm. **b**, **d** The measurement of wound area in MCF-7 and HepG2, respectively, shows that it remains almost unaffected in cells treated with the tested complexes. This indicates their ability to inhibit cancer cell migration, especially complex (**2**). The values presented here are the mean ± standard deviation (SD) of three independent studies. Scale bar: 1 mm
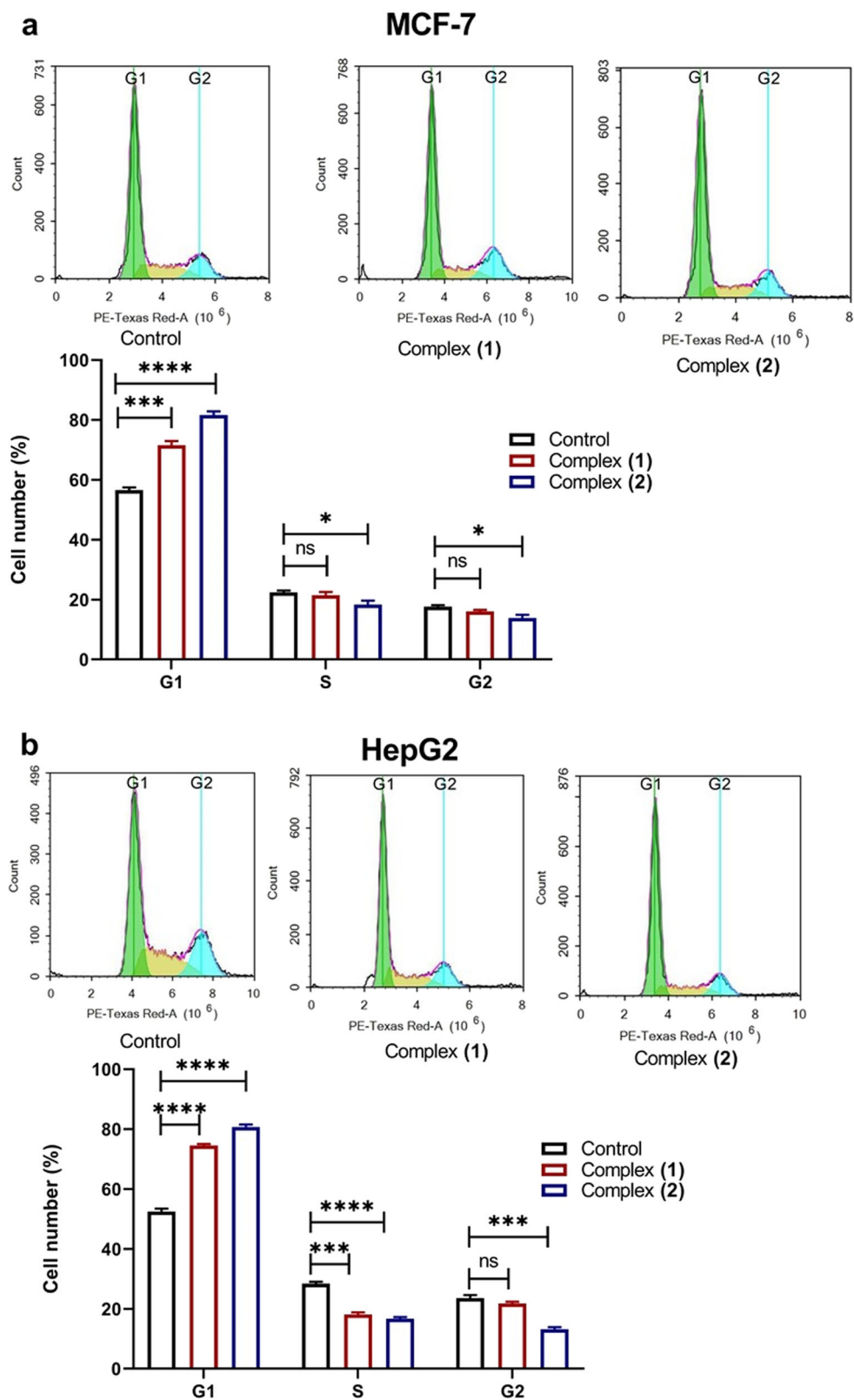
Fig. 7 Cell cycle study in breast cancer and liver cancer cells using the tested complexes. **a** MCF-7 was exposed to both complexes (**1**) and (**2**) for 72 h, stained with PI for DNA content, and assessed by flow cytometry. **b** HepG2 was exposed to both complexes (**1**) and (**2**) for 72 h, stained with PI for DNA content, and assessed by flow cytometry. Data are displayed as mean ± SD for three experiment repeats. Significant differences exist between the experimental group and the control group, as indicated by the following: ns = non-significant, *$P < 0.05$, ***$P < 0.001$, and ****$P < 0.0001$ levels

proliferation, leading to cancer. Induction of apoptosis is one of the major mechanisms by which antitumor agents induce tumor cell death [65]. RT-PCR analysis of genes associated with apoptosis indicated that Cu (II) complexes (1) and (2) activate apoptosis by triggering BAX, p53, and Caspase 3 while inhibiting the anti-apoptotic gene Bcl2. In different cell lines, the mRNA levels for these selected genes were measured after 24, 48, and 72 h of treatment at IC_{50} concentrations of both tested complexes. As shown in Fig. 9, complex (2) exhibits a higher apoptotic activity on both cancer cell lines and a lower activity on the HSF cell line than complex (1). Therefore, complex (2) could initiate a natural cell death mechanism, preventing cancer cells from proliferating and not affecting normal cells. Apoptosis increased 5-fold and 6-fold in the p53 and BAX genes after 24 h of treatment with complex (2). After 48 h of complex (2) treatment, p53 and BAX genes increased 10-fold and 15-fold, respectively, and 15-fold and 20-fold after 72 h of complex (2) treatment, respectively, in comparison with the control (Fig. 9b). This elevation was significantly higher than in complex (1). These were 3-fold and 5-fold expression folds in p53 and BAX genes at 24 h, while at 48 h, the expression folds for p53 and BAX were 7-fold and 11-fold, and at 72 h, the folds were 12-fold and 14-fold for p53 as well as BAX genes in breast cancer cells (MCF-7) (Fig. 9a). Complex (2) causes liver cancer cells to undergo more apoptosis than breast cancer cells (Fig. 9d). In 24 h, the folds were 9-fold, 15-fold, and 4-fold in p53, BAX, and Caspase 3, respectively, while in 48 h, they were 19-fold, 23-fold, and 13-fold. At 72 h, the p53, BAX, and Caspase 3 folds were 27, 31, and 18, respectively. Complex (1) had a lower effect on HepG2 than complex (2) at 24 h; the folds were 4, 5, and 3 for p53, BAX, and Caspase 3, respectively; 13, 17, and 11 at 48 h; and 15, 20, and 13 for p53, BAX, and Caspase 3, respectively, at 72 h (Fig. 9c). Synthesized Cu (II) complexes indicate that cellular DNA content has been fragmented and bound to DNA. Additionally, the anti-apoptotic percentage (Bcl2) decreased in HepG2 and MCF-7 cells exposed to complex (2) to nearly 55% compared to cancer cells untreated. Compared to the control, the anti-apoptotic percentage (Bcl2) decreased by 45% with complex (1). In normal cells (HSF), complex (2) (Fig. 9e) had lower effects on the expression of tested genes than complex (1) (Fig. 9f), consistent with results obtained from anticancer assays.

Cytotoxic drugs inhibit cancer cell proliferation by cell cycle arrest, apoptosis, or a combination of both [66]. Apoptosis is a form of programmed cell death that activates an internal mechanism, triggering several signal transmission routes to destroy the cell ultimately. This process can occur in both pathological and nonpathological circumstances [67, 68]. There are two primary apoptotic pathways: the extrinsic apoptotic system, which is handled by cell death receptors, and the intrinsic apoptotic pathway, which is mediated by mitochondria. The Bcl2 family comprises the primary proteins responsible for controlling apoptosis. They are predominantly situated within the mitochondria and linked to cytochrome c's liberation [69].

In this investigation, we found that the mRNA levels of the tumor-suppressor gene p53 and the apoptotic genes BAX and Caspase 3 were increased. In contrast, the expression of the anti-apoptotic gene Bcl2 was decreased in MCF-7 and HepG2 cells treated with synthesized Cu (II) complexes. An increase in the level of p53 expression causes the activation of pro-apoptotic Bcl2 family members, such as BAX, which results in the permeation of the outer mitochondrial membrane. This leads to the release of soluble proteins from the intermembrane gap into the cytosol, where they facilitate the activation of Caspase [70].

Fan et al. [71] examined the impact of Metam/Cu (II) on HepG2 cells. The findings demonstrated that Metam/Cu (II) elevated the protein expression ratio of BAX/Bcl2. Multiple studies have shown that certain Cu (II) complexes can enhance the expression of the BAX/Bcl2 ratio in different cancer cell lines, including MCF-7 and BEL-7404 cells. These findings suggest that the Bcl2 family of proteins may trigger apoptosis through Cu (II) complexes. Consistent with our findings, Zhu et al. [13] showed that a Cu (II) combination of a coumarin derivative increased the expression of P53 and BAX while decreasing the expression of Bcl2. P53 activation has a pro-apoptotic function as it stimulates and reduces the expression of specific essential cell death effectors, resulting in apoptotic cell death.

Prior studies have indicated that P53 enhances the expression of the BAX gene, which belongs to the pro-apoptotic members of the Bcl2 family while suppressing the expression of the Bcl2 gene, an anti-apoptotic gene within the same family.

Thus, in the current investigation, BAX gene expression was notably increased in MCF-7 and HepG2 cells under treatment time conditions (Fig. 9). The Bcl2 gene expression levels in MCF-7 and HepG2 cells were markedly reduced after 24, 48, and 72 h of treatment. Conversely, Caspase 3 was dramatically upregulated under the circumstances of treatment duration (Fig. 9).

The BAX gene is a member of the Bcl2 family that promotes programmed cell death (apoptosis). It is produced in the cytosol when cells are exposed to apoptotic stressors, such as cytotoxic medicines. The BAX protein mediates programmed cell death and moves from the cytosol to the mitochondria. This movement leads to apoptosis after cytochrome c release from the mitochondria.
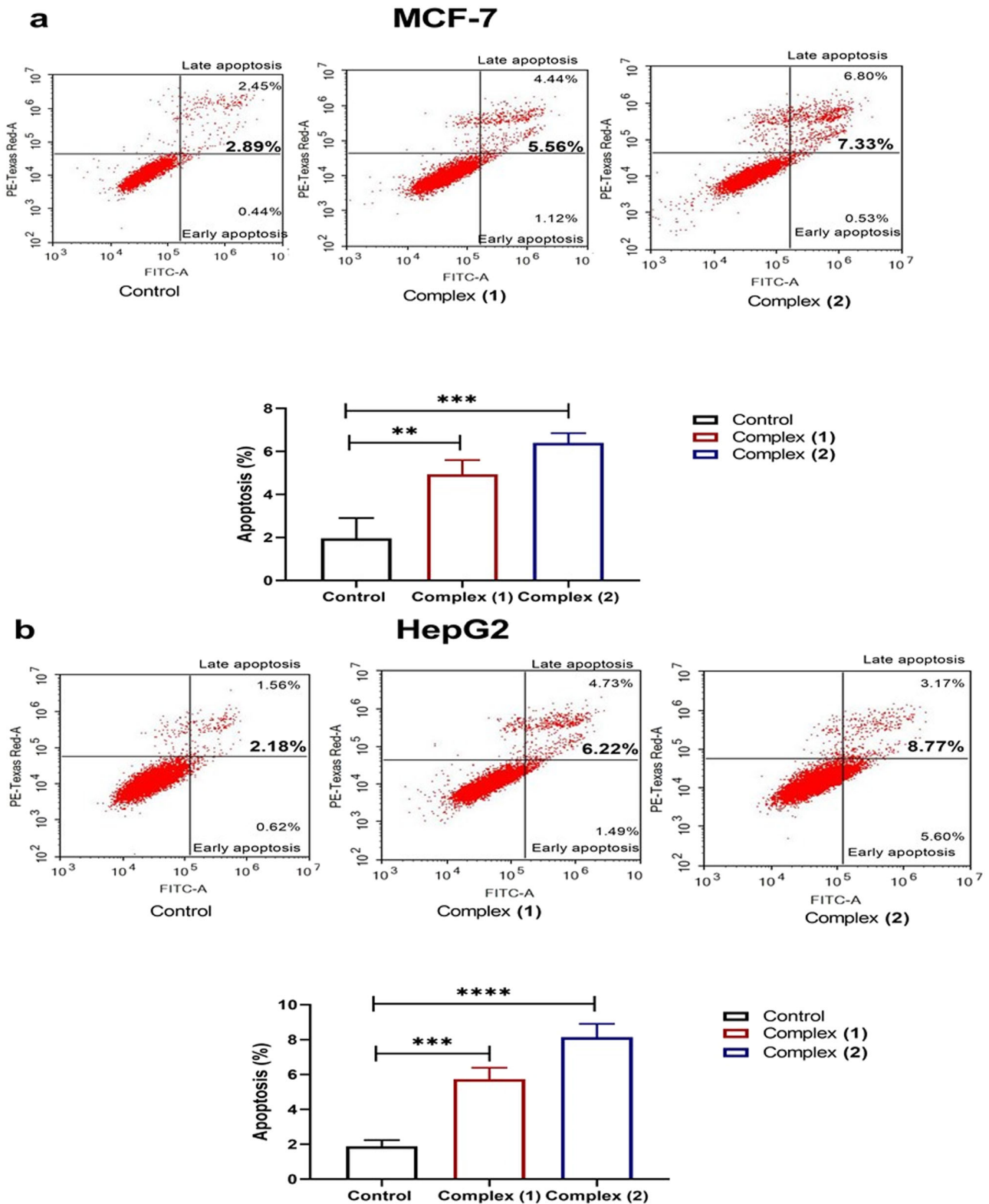
Fig. 8 The effect of the tested Cu (II) complexes on MCF-7 and HepG2 cell apoptosis rates after incubation with the target complexes for 72 h. **a** Apoptosis was monitored by flow cytometry by treating MCF-7 cells with both complexes (**1**) and (**2**) and staining them with Annexin V-FITC/PI. **b** After HepG2 cells were exposed to both complexes (**1**) and (**2**) and stained with Annexin V-FITC/PI, flow cytometry was utilized to measure apoptosis. For three repeated experiments, the findings were presented as the mean ± SD. The significance levels are **$P < 0.01$, ***$P < 0.001$, and ****$P < 0.0001$
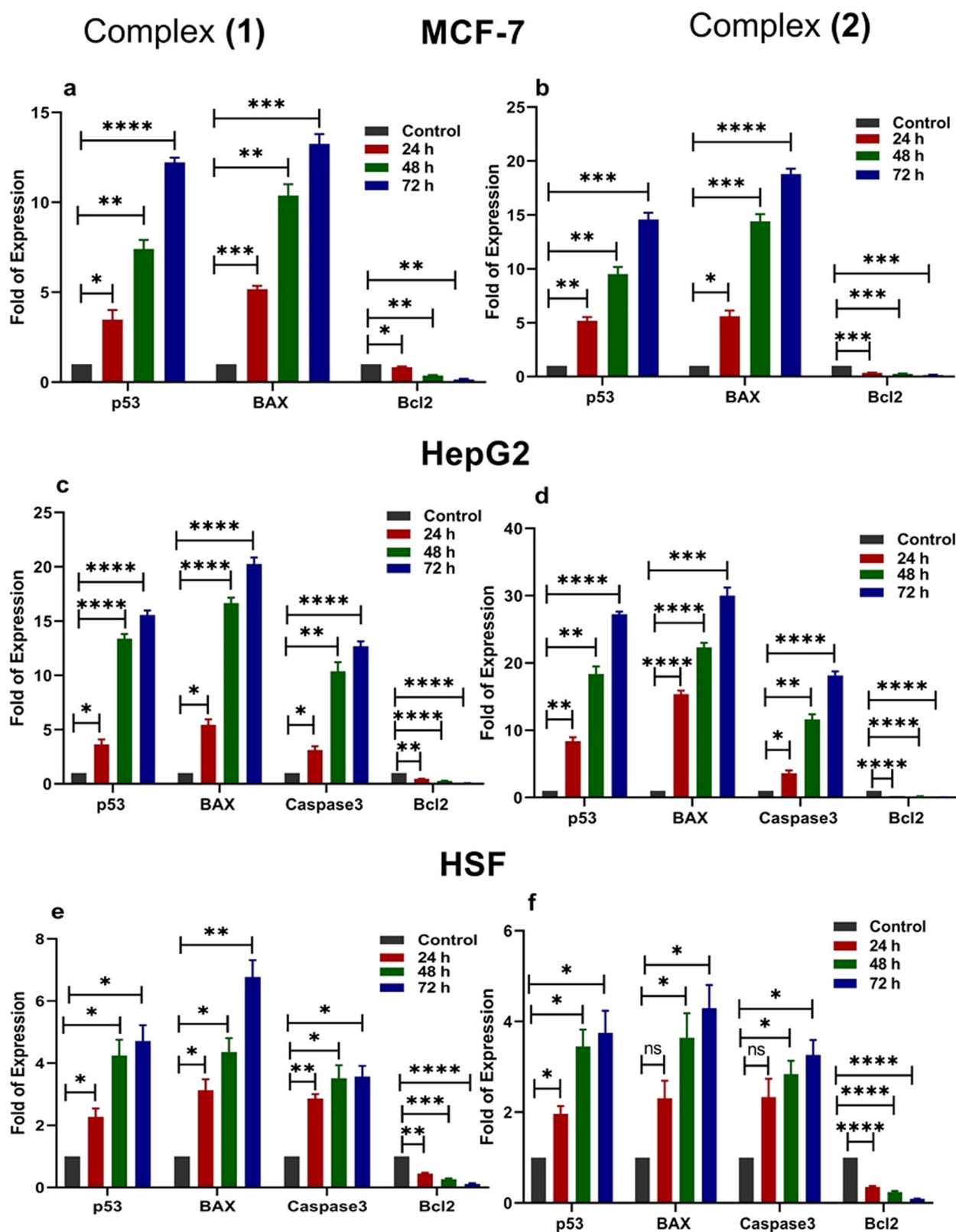
Fig. 9 Influence of the prepared Cu (II) complexes on gene expression using RT-PCR analysis to evaluate the expression levels of p53, BAX, Caspase 3, and Bcl2 in breast cancer where (**a**) is complex (1) and (**b**) is complex (2), liver cancer where (**c**) is complex (1) and (**d**) is complex (2), and human skin fibroblast cells where (**e**) is complex (1) and (**f**) is complex (2) at the IC_{50}s after 24, 48, and 72 h of treatment with the tested complexes. β-actin worked as an internal control. Data are displayed as the mean ± SD. The data points represent the average of separate studies conducted in triplicate. *$P < 0.05$, **$P < 0.01$, ***$P < 0.001$, and ****$P < 0.0001$ represent a significant difference relative to control cells
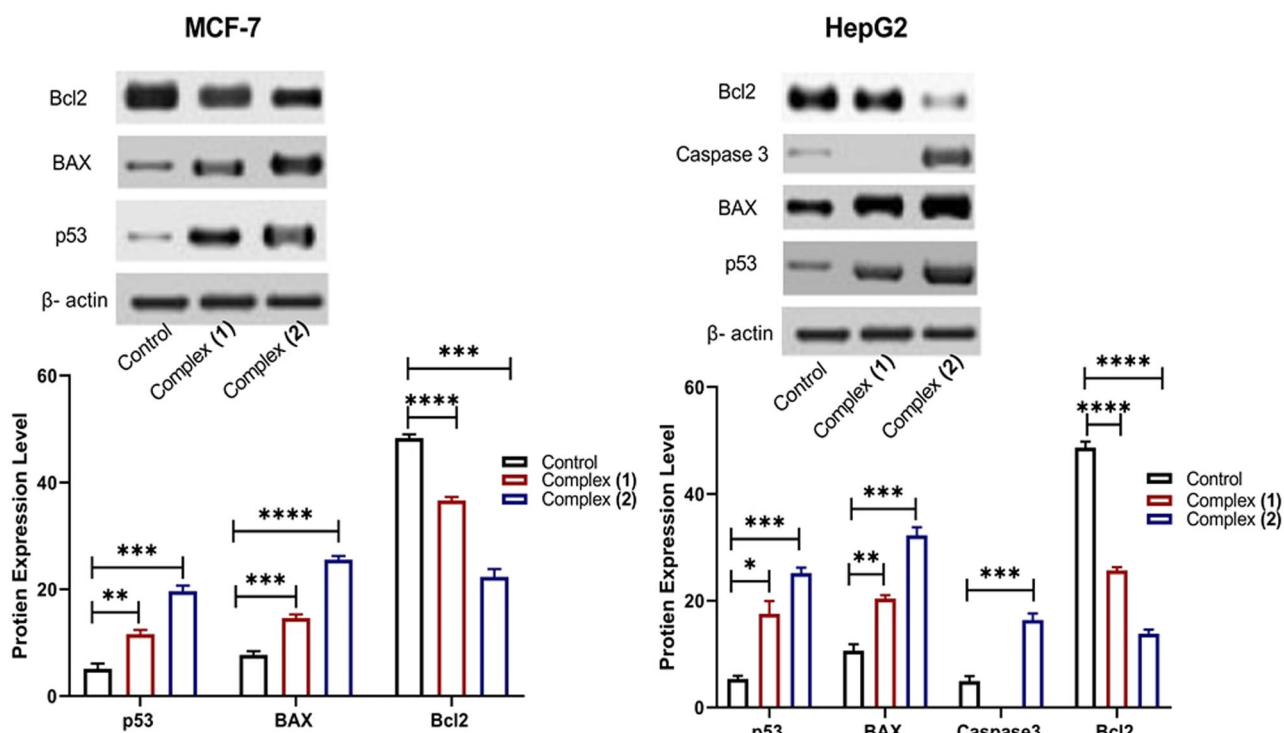
Fig. 10 In breast cancer and liver cancer cell lines, the effect of Cu (II) complexes was investigated on the protein expression of p53, BAX, Caspase 3, and Bcl2. For 72 h, cancer cells were treated with the prepared Cu (II) complexes at their respective IC_{50} values. Protein expression levels were assessed by densitometric analysis of the two autoradiographies. Data are presented as mean ± SD. Each data point is the average of three repeated studies. $*P < 0.05$, $**P < 0.01$, $***P < 0.001$, and $****P < 0.0001$ met the statistical significance criteria

In this investigation, we showed that the BAX/Bcl2 ratio was elevated in MCF-7 and HepG2 cells when exposed to Cu (II) complexes (**1**) and (**2**) for 24, 48, and 72 h (Fig. S3). BAX and Bcl2 play a role in the intrinsic apoptosis pathway, which is not dependent on Caspase activation or the extrinsic pathway of programmed cell death. The suppression of Bcl2 leads to the relocation of BAX to the mitochondria and initiates the intrinsic apoptotic pathway after treating MCF-7 and HepG2 cells with the complex at the IC_{50} concentration.

The findings of the current experiment demonstrated that the examined Cu (II) complexes (**1**) and (**2**) induced apoptosis in MCF-7 and HepG2 cells through both extrinsic and intrinsic apoptotic mechanisms. However, further investigation is required to validate this, which will be conducted in our next in vivo study.

Figure S3. The effect of Cu (II) complexes (**1**) and (**2**) on the BAX/Bcl2 mRNA ratio. RT-PCR analysis detected BAX/Bcl2 mRNA expression in MCF-7 and HepG2 cells at IC_{50} concentrations after 24, 48, and 72 h treatment with the tested complexes. Data are represented as mean ± SD. Each data point is an average of results obtained from three independent experiments performed in triplicate. $*P < 0.05$, $**P < 0.01$, $***P < 0.001$, and $****P < 0.0001$ indicate a significant difference with the control cells.

Western Blot Assay

As shown in Fig. 10, protein expression supports our gene expression findings. Pro-apoptotic gene expression is upregulated, and anti-apoptotic gene expression is down-regulated in treated cancer cell lines compared to control cells. Tumor suppressor genes p53, BAX, and Caspase 3 are significantly upregulated. Moreover, Bcl2 oncogene expression is strongly inhibited, suggesting that synthesized Cu (II) complexes, especially complex (**2**), may also target oncogenes. The reduction in Bcl2 expression could indicate that tumor cell lines may enter the apoptotic pathway. The expression pattern of the tested proteins matches gene expression and anticancer activity in vitro. A molecular docking analysis was conducted to learn more about how the tested Cu (II) complexes interact with the Bcl2 inhibitor.

Molecular Docking

In this study, the synthesized Cu (II) complexes, especially complex (**2**), displayed antiproliferative effects against MCF-7 and HepG2 cells via apoptosis. The molecular modeling approach was applied to assess how the complexes bind with the anti-apoptotic protein Bcl2 (PDB ID: 4IEH), which confirmed the experimental results. The

Chimera score indicated that complex (2) had a maximum binding affinity for Bcl2 ($\Delta G = -7.20$), while complex (1) had a minimum binding affinity ($\Delta G = -6.60$). This means that complex (2) affects Bcl2 more strongly than complex (1). The docking analysis indicates the formation of two hydrogen bonds within the complex (1) as well as Bcl2 via C=O…O of ASP 61 A with a distance of 3.41 Å and C=O…O of SER 64 A with a distance of 2.98 Å (Fig. S4a). Complex (2) and Bcl2 formed two hydrogen bonds via N-H…O of ASP 31 A with a distance of 2.14 Å; the other hydrogen bond was formed via C=O…N-H of ARG 12 A with a distance of 3.34 Å (Fig. S4b). The docking results for the tested complexes correlate with anticancer, flow cytometry, gene expression, and protein expression. This shows the strong effect of complex (2) on cancer cells.

Fig. S4. Molecular docking simulation of the tested Cu complexes with Bcl2 (PDB ID: 4IEH), where (a) is complex (1) and (b) is complex (2).

Conclusion

The present work presents an extensive study of the cytotoxic efficacy of Cu (II) complexes by exploiting the selective permeability of the cancer cell membrane to accumulate Cu (II), which significantly destroys cancer cells [72]. Triflupromazine also plays a crucial role in enhancing anticancer activity by inhibiting cancer cell growth primarily through disrupting the cell membrane, damaging DNA, and triggering pro-apoptotic genes to arrest cell cycles that lead to cell death [73].

In this study, the biological applications and cytotoxic potential of ternary Cu (II) complexes involving triflupromazine coupled to glycine and histidine were extensively studied. Cyclic voltammetry was applied to evaluate DNA-Cu (II) complexes' interactions, which revealed strong binding to CT-DNA. The tested complexes bind to DNA electrostatically. Compared to complex (1), complex (2) showed superior biological activity in viral and parasite treatments. It also prevented inflammation of human red blood cells, in addition to promising cytotoxic activity in MCF-7 and HepG2 cancer cell lines with low IC_{50}s of 40.25 and 35.36 μg/mL, respectively. Complex (2) also exhibited promising accumulation in HepG2 cells, as described in the cellular drug uptake assay. It was found to be safe on a normal HSF cell line with a high IC_{50} value of 182.84 μg/mL. The results of cell cycle arrest studies indicate that complex (2) prevents proliferation in cancer cells during the G1 phase. Complex (2) showed potent apoptotic activity in treated cancer cells labeled with Annexin V-FITC/PI stain.

Furthermore, the molecular docking study confirmed the potential binding activity of both complexes, with special emphasis on complex (2) of the Bcl2 inhibitor. This is in agreement with the gene expression and western blot results, which demonstrate the upregulation of the pro-apoptotic genes and the downregulation of the anti-apoptotic genes. The higher anticancer efficacy of complex (2) could be attributed to the imidazole ring in histidine. This ring causes significant deformation of the DNA double helix in cancer cells and inhibits replication, transcription, cell growth, and cell division [74]. It enhances the apoptosis pathway by activating pro-apoptotic genes, as observed in the above gene expression and western blot assays (Figs. 9 and 10).

The biological outcomes obtained from complex (2) show promise for future in vivo studies using an animal model to develop novel anticancer agents.

Author Contributions All authors contributed to the study's conception and design. Material preparation, data collection, and analysis were performed by Nourhan S. Sultan, Azza A. Shoukry, Fatma B. Rashidi, and Heba K. Abdelhakim. The first draft of the manuscript was written by Nourhan S. Sultan and all authors commented on previous versions of the manuscript. All authors read and approved the final manuscript. Nourhan S. Sultan: Methodology, Investigation, Validation, Software, Writing-Original draft preparation. Azza A. Shoukry: Supervision, Conceptualization, Problem orientation, Investigation, Reviewing. Fatma B. Rashidi: Supervision, Conceptualization, Problem orientation, Investigation, Reviewing Heba K. Abdelhakim: Supervision, Conceptualization, Problem orientation, Investigation, Reviewing.

Compliance with Ethical Standards

Conflict of interest The authors declare no competing interests.

References

1. Selvam, P., De, S., Paira, P., Kumar, S. K. A., Kumar R, S., Moorthy, A., Ghosh, A., Kuo, Y.-C., Banerjee, S., & Jenifer, S. K. (2022). In vitro studies on the selective cytotoxic effect of luminescent Ru(ii)-p-cymene complexes of imidazo-pyridine and imidazo quinoline ligands. *Dalton Transactions*, *51*(45), 17263–17276.

2. Jia, L., Xu, J., Zhao, X., Shen, S., Zhou, T., Xu, Z., Zhu, T., Chen, R., Ma, T., Xie, J., Dong, K., & Huang, J. (2016). Synthesis, characterization, and antitumor activity of three ternary dinuclear copper (II) complexes with a reduced Schiff base ligand and diimine coligands in vitro and in vivo. *Journal of Inorganic Biochemistry*, *159*, 107–119.

3. Kucková, L., Jomová, K., Švorcová, A., Valko, M., Segľa, P., Moncoľ, J., & Kožíšek, J. (2015). Synthesis, crystal structure, spectroscopic properties and potential biological activities of salicylate–neocuproine ternary copper(II) complexes. *Molecules*, *20*, 2115–2137. https://doi.org/10.3390/molecules20022115.

4. De, S., & Ashok Kumar, S. K. (2020). Development of highly potent Arene-Ru (II)-ninhydrin complexes for inhibition of cancer cell growth. *Inorganica Chimica Acta*, *508*, 119641.

5. Kelland, L. (2007). The resurgence of platinum-based cancer chemotherapy. *Nature Reviews Cancer*, *7*(8), 573–584.

6. Iglesias, S., Alvarez, N., Torre, M. H., Kremer, E., Ellena, J., Ribeiro, R. R., Barroso, R. P., Costa-Filho, A. J., Kramer, M. G., & Facchin, G. (2014). Synthesis, structural characterization and cytotoxic activity of ternary copper(II)–dipeptide–phenanthroline complexes. A step towards the development of new copper compounds for the treatment of cancer. *Journal of Inorganic Biochemistry, 139*, 117–123.

7. Bhatt, B. S., Gandhi, D. H., Vaidya, F. U., Pathak, C., & Patel, T. N. (2021). Cell apoptosis induced by ciprofloxacin based Cu(II) complexes: cytotoxicity, SOD mimic and antibacterial studies. *Journal of Biomolecular Structure and Dynamics, 39*(12), 4555–4562.

8. Gandhi, D. H., Vaidya, F. U., Pathak, C., Patel, T. N., & Bhatt, B. S. (2022). Mechanistic insight of cell anti-proliferative activity of fluoroquinolone drug-based Cu(II) complexes. *Molecular Diversity, 26*(2), 869–878.

9. Varma, R. R., Pandya, J. G., Vaidya, F. U., Pathak, C., Bhatt, B. S., & Patel, M. N. (2020). Biological activities of pyrazoline-indole based Re(I) carbonyls: DNA interaction, antibacterial, anticancer, ROS production, lipid peroxidation, in vivo *and* in vitro *cytotoxicity studies*. *Chemico-Biological Interactions, 330*, 109231.

10. Arumugham, M. N. (2013). Synthesis, characterisation, DNA-binding studies and antimicrobial activity of copper(II) complex with 1,10 phenanthroline, L-tyrosine and urea as ligands. *International Journal of Inorganic and Bioinorganic Chemistry, 3*, 8–15.

11. Patel, M. N., Bhatt, B. S., & Dosi, P. A. (2012). Study of SOD mimic and nucleic acid interaction activity exerted by enrofloxacin-based copper(II) complexes. *Chemistry & Biodiversity, 9*(12), 2810–2824.

12. Li, X., Bi, C.-F., Fan, Y.-H., Zhang, X., Meng, X.-M., & Cui, L.-S. (2014). Synthesis, crystal structure and anticancer activity of a novel ternary copper(II) complex with Schiff base derived from 2-amino-4-fluorobenzoic acid and salicylaldehyde. *Inorganic Chemistry Communications, 50*, 35–41.

13. Zhu, T., Chen, R., Yu, H., Feng, Y., Chen, J., Lu, Q., Xie, J., Ding, W., & Ma, T. (2014). Antitumor effect of a copper (II) complex of a coumarin derivative and phenanthroline on lung adenocarcinoma cells and the mechanism of action. *Molecular Medicine Reports, 10*(5), 2477–2482.

14. Chen, L., Dong, W.-K., Zhang, H., Zhang, Y., & Sun, Y.-X. (2017). Structural variation and luminescence properties of tri- and dinuclear CuII and ZnII complexes constructed from a naphthalenediol-based bis(salamo)-type ligand. *Crystal Growth & Design, 17*(7), 3636–3648.

15. Mahmoud, W. H., Mohamed, G. G., & El-Dessouky, M. M. I. (2015). Synthesis, structural characterization, in vitro anti-microbial and anticancer activity studies of ternary metal complexes containing glycine amino acid and the anti-inflammatory drug lornoxicam. *Journal of Molecular Structure, 1082*, 12–22.

16. Grosser, N., Oberle, S., Berndt, G., Erdmann, K., Hemmerle, A., & Schröder, H. (2004). Antioxidant action of l-alanine: heme oxygenase-1 and ferritin as possible mediators. *Biochemical and Biophysical Research Communications, 314*(2), 351–355.

17. Borisz, V., ÁKos, C., Andrea, C., Joseph, M., Leonard, A., & Gabriella, S. (2017). Possible biological and clinical applications of phenothiazines. *Anticancer Research, 37*(11), 5983 p.

18. Środa-Pomianek, K., Michalak, K., Świątek, P., Poła, A., Palko-Łabuz, A., & Wesołowska, O. (2018). Increased lipid peroxidation, apoptosis and selective cytotoxicity in colon cancer cell line LoVo and its doxorubicin-resistant subline LoVo/Dx in the presence of newly synthesized phenothiazine derivatives. *Biomedicine & Pharmacotherapy, 106*, 624–636.

19. Kumar, V., Upadhyay, N., & Manhas, A. (2015). Designing, syntheses, characterization, computational study and biological activities of silver-phenothiazine metal complex. *Journal of Molecular Structure, 1099*, 135–141.

20. Colqui Quiroga, M. V., Monzón, L. M. A., & Yudi, L. M. (2010). Interaction of triflupromazine with distearoylphosphatidylglycerol films studied by surface pressure isotherms and cyclic voltammetry at a 1,2-dichloroethane/water interface. *Electrochimica Acta, 55*(20), 5840–5846.

21. Chou, F. H.-C., Tsai, K.-Y., Su, C.-Y., & Lee, C.-C. (2011). The incidence and relative risk factors for developing cancer among patients with schizophrenia: A nine-year follow-up study. *Schizophrenia Research, 129*(2), 97–103.

22. Tabarés-Seisdedos, R., & Rubenstein, J. L. (2013). Inverse cancer comorbidity: a serendipitous opportunity to gain insight into CNS disorders. *Nature Reviews Neuroscience, 14*(4), 293–304.

23. Jaszczyszyn, A., Gąsiorowski, K., Świątek, P., Malinka, W., Cieślik-Boczula, K., Petrus, J., & Czarnik-Matusewicz, B. (2012). Chemical structure of phenothiazines and their biological activity. *Pharmacological Reports, 64*(1), 16–23.

24. Sultan, N. S., Elhakim, H. K. A., Shoukry, A. A., & Rashidi, F. B. (2023). Synthesis, characterization, and biological evaluation of Cu(II) complexes containing triflupromazine with glycine and histidine. *Chemistry & Biodiversity, n/a*(n/a), e202300450.

25. Donalisio, M., Nana, H. M., Ngono Ngane, R. A., Gatsing, D., Tiabou Tchinda, A., Rovito, R., Cagno, V., Cagliero, C., Boyom, F. F., Rubiolo, P., Bicchi, C., & Lembo, D. (2013). In vitro anti-Herpes simplex virus activity of crude extract of the roots of Nauclea latifolia Smith (Rubiaceae). *BMC Complementary and Alternative Medicine, 13*(1), 266.

26. Vichai, V., & Kirtikara, K. (2006). Sulforhodamine B colorimetric assay for cytotoxicity screening. *Nature Protocols, 1*(3), 1112–1116.

27. Pauwels, R., Balzarini, J., Baba, M., Snoeck, R., Schols, D., Herdewijn, P., Desmyter, J., & De Clercq, E. (1988). Rapid and automated tetrazolium-based colorimetric assay for the detection of anti-HIV compounds. *Journal of Virological Methods, 20*(4), 309–321.

28. Zandi, K., Zadeh, M. A., Sartavi, K. & Rastian, Z. (2007). Antiviral activity of Aloe vera against herpes simplex virus type 2: An in vitro study. *African Journal of Biotechnology*. 6 (15).

29. Al-salahi, R., Al-Swaidan, I., Al-Omar, M., & Marzouk, M. (2013). Antiviral activity of 2-phenoxy-[1,2,4]triazolo[1,5-α]quinazoline derivatives. *Life Science Journal, 10*, 2164–2169.

30. Vila-Nova, N. S., de Morais, S. M., Falcão, M. J. C., Alcantara, T. T. N., Ferreira, P. A. T., Cavalcanti, E. S. B., Vieira, I. G. P., Campello, C. C., & Wilson, M. (2013). Different susceptibilities of Leishmania spp. promastigotes to the Annona muricata acetogenins annonacinone and corossolone, and the Platymiscium floribundum coumarin scoparone. *Experimental Parasitology, 133*(3), 334–338. p.

31. Tritten, L., Nwosu, U., Vargas, M., & Keiser, J. (2012). In vitro *and* in vivo efficacy of tribendimidine and its metabolites alone and in combination against the hookworms Heligmosomoides bakeri and Ancylostoma ceylanicum. *Acta Tropica, 122*(1), 101–107.

32. Abou Rayia, D. M., Saad, A. E., Ashour, D. S., & Oreiby, R. M. (2017). Implication of artemisinin nematocidal activity on experimental trichinellosis: In vitro *and* in vivo *studies*. *Parasitology International, 66*(2), 56–63.

33. Bughdadi, F. A. (2010). Ultrastructural studies on the parasitic worm Trichinella Spiralis. *Journal of Taibah University for Science, 3*(1), 33–38.

34. Anosike, C. A., Obidoa, O., & Ezeanyika, L. U. S. (2012). Membrane stabilization as a mechanism of the anti-inflammatory activity of methanol extract of garden egg (Solanum aethiopicum). *DARU Journal of Pharmaceutical Sciences, 20*(1), 76.

35. Orellana, E. A., & Kasinski, A. L. (2016). Sulforhodamine B (SRB) assay in cell culture to investigate cell proliferation. *Bio-protocol, 6*(21), e1984–e1984.

36. Hu, W., Fang, L., Hua, W., & Gou, S. (2017). Biotin-Pt (IV)-indomethacin hybrid: A targeting anticancer prodrug providing enhanced cancer cellular uptake and reversing cisplatin resistance. *Journal of Inorganic Biochemistry*, *175*, 47–57.

37. Lie, M. R. K. L., van der Giessen, J., Fuhler, G. M., de Lima, A., Peppelenbosch, M. P., van der Ent, C., & van der Woude, C. J. (2018). Low dose Naltrexone for induction of remission in inflammatory bowel disease patients. *Journal of Translational Medicine*, *16*(1), 55.

38. Fekry, M. I., Ezzat, S. M., Salama, M. M., Alshehri, O. Y., & Al-Abd, A. M. (2019). Bioactive glycoalkaloides isolated from Solanum melongena fruit peels with potential anticancer properties against hepatocellular carcinoma cells. *Scientific Reports*, *9*(1), 1746.

39. Bashmail, H. A., Alamoudi, A. A., Noorwali, A., Hegazy, G. A., AJabnoor, G., Choudhry, H., & Al-Abd, A. M. (2018). Thymoquinone synergizes gemcitabine anti-breast cancer activity via modulating its apoptotic and autophagic activities. *Scientific Reports*, *8*(1), 1–11.

40. Rezaei, A., Mahmoodi, M., Mohammadizadeh, F., Mohamadi, M., Hajizadeh, M. R., Mirzaei, M. R., & Khanamani Falahati-Pour, S. (2019). A novel copper (II) complex activated both extrinsic and intrinsic apoptotic pathways in liver cancerous cells. *Journal of Cellular Biochemistry*, *120*(8), 12280–12289.

41. Biswas, N., Khanra, S., Sarkar, A., Bhattacharjee, S., Prasad Mandal, D., Chaudhuri, A., Chakraborty, S., & Roy Choudhury, C. (2017). One new azido bridged dinuclear copper(ii) thiosemicarbazide complex: synthesis, DNA/protein binding, molecular docking study and cytoxicity activity. *New Journal of Chemistry*, *41*(21), 12996–13011.

42. Morris, G. M., Huey, R., Lindstrom, W., Sanner, M. F., Belew, R. K., Goodsell, D. S., & Olson, A. J. (2009). AutoDock4 and AutoDockTools4: automated docking with selective receptor flexibility. *Journal of Computational Chemistry*, *30*(16), 2785–2791.

43. De, A., Ray, H. P., Jain, P., Kaur, H., & Singh, N. (2020). Synthesis, characterization, molecular docking and DNA cleavage study of transition metal complexes of o-vanillin and glycine-derived Schiff base ligand. *Journal of Molecular Structure*, *1199*, 126901.

44. Aslanoglu, M. (2006). Electrochemical and spectroscopic studies of the interaction of proflavine with DNA. *Analytical Sciences*, *22*(3), 439–443.

45. Li, N., Ma, Y., Yang, C., Guo, L., & Yang, X. (2005). Interaction of anticancer drug mitoxantrone with DNA analyzed by electrochemical and spectroscopic methods. *Biophysical Chemistry*, *116*(3), 199–205.

46. Shah, A., Zaheer, M., Qureshi, R., Akhter, Z., & Faizan Nazar, M. (2010). Voltammetric and spectroscopic investigations of 4-nitrophenylferrocene interacting with DNA. *Spectrochimica Acta Part A: Molecular and Biomolecular Spectroscopy*, *75*(3), 1082–1087.

47. Otręba, M., Kośmider, L., & Rzepecka-Stojko, A. (2020). Antiviral activity of chlorpromazine, fluphenazine, perphenazine, prochlorperazine, and thioridazine towards RNA-viruses. A review. *European Journal of Pharmacology*, *887*, 173553.

48. Hart, B. J., Dyall, J., Postnikova, E., Zhou, H., Kindrachuk, J., Johnson, R. F., Olinger, Jr, G. G., Frieman, M. B., Holbrook, M. R., & Jahrling, P. B. (2014). Interferon-β and mycophenolic acid are potent inhibitors of Middle East respiratory syndrome coronavirus in cell-based assays. *The Journal of General Virology*, *95*(Pt 3), 571.

49. Zeng, Z., Zhang, R., Hong, W., Cheng, Y., Wang, H., Lang, Y., Ji, Z., Wu, Y., Li, W., & Xie, Y. (2018). Histidine-rich modification of a scorpion-derived peptide improves bioavailability and inhibitory activity against HSV-1. *Theranostics*, *8*(1), 199.

50. Shalaby, M. A., Moghazy, F. M., Shalaby, H. A., & Nasr, S. M. (2010). Effect of methanolic extract of Balanites aegyptiaca fruits on enteral and parenteral stages of Trichinella spiralis in rats. *Parasitology Research*, *107*(1), 17–25.

51. Yadav, A. K., & Temjenmongla (2012). Efficacy of Lasia spinosa leaf extract in treating mice infected with Trichinella spiralis. *Parasitology Research*, *110*(1), 493–498.

52. Djurković-Djaković, O., Bobić, B., Nikolić, A., Klun, I., & Dupouy-Camet, J. (2013). Pork as a source of human parasitic infection. *Clinical Microbiology and Infection*, *19*(7), 586–594.

53. Abdul Wahab, S. M., Jantan, I., Haque, M. A., & Arshad, L. (2018). Exploring the leaves of *Annona muricata L.* as a source of potential anti-inflammatory and anticancer agents. *Frontiers in Pharmacology*, *9*, 661.

54. Lacey, E. (1990). Mode of action of benzimidazoles. *Parasitology Today*, *6*(4), 112–115.

55. Gunathilake, K. D. P. P., Ranaweera, K. K. D. S. & Rupasinghe, H. P. V. (2018). In vitro anti-inflammatory properties of selected green leafy vegetables. Biomedicines. **6**, https://doi.org/10.3390/biomedicines6040107.

56. Aiyelabola, T. O. (2021). Syntheses, characterization and biological activity of novel thiazoylazo dye and its coordination compounds. *Advances in Biological Chemistry*, *11*(5), 179–205.

57. Mohanraj, M., Ayyannan, G., Raja, G., & Jayabalakrishnan, C. (2017). Synthesis, characterization and in vitro biological assays of copper(II) and nickel(II) complexes with furan-2-carboxylic acid hydrazide. *Applied Organometallic Chemistry*, *31*(4), e3582.

58. Franz, C. M., Jones, G. E., & Ridley, A. J. (2002). Cell migration in development and disease. *Developmental Cell*, *2*(2), 153–158.

59. Nagababu, P., Barui, A. K., Thulasiram, B., Devi, C. S., Satyanarayana, S., Patra, C. R., & Sreedhar, B. (2015). Antiangiogenic activity of mononuclear copper(II) polypyridyl complexes for the treatment of cancers. *Journal of Medicinal Chemistry*, *58*(13), 5226–5241.

60. Stuelten, C. H., Parent, C. A., & Montell, D. J. (2018). Cell motility in cancer invasion and metastasis: insights from simple model organisms. *Nature Reviews Cancer*, *18*(5), 296–312.

61. Ali, I., Lone, M. N., & Aboul-Enein, H. Y. (2017). Imidazoles as potential anticancer agents. *MedChemComm*, *8*(9), 1742–1773.

62. Nayak, S., Gaonkar, S. L., Musad, E. A., & Dawsar, A. M. A. L. (2021). 1,3,4-Oxadiazole-containing hybrids as potential anticancer agents: Recent developments, mechanism of action and structure-activity relationships. *Journal of Saudi Chemical Society*, *25*(8), 101284.

63. Wang, X., Li, Y., Gong, S., & Fu, D. (2002). A spectroscopic study on the dna binding behavior of the anticancer drug dacarbazine. *Spectroscopy Letters*, *35*(6), 751–756.

64. Chatterjee, S., Kundu, S., Bhattacharyya, A., Hartinger, C. G., & Dyson, P. J. (2008). The ruthenium(II)–arene compound RAPTA-C induces apoptosis in EAC cells through mitochondrial and p53–JNK pathways. *Journal of Biological Inorganic Chemistry*, *13*(7), 1149–1155.

65. El-Afify, M. E., Elsayed, S. A., Shalaby, T. I., Toson, E. A., & El-Hendawy, A. M. (2021). Synthesis, characterization, DNA binding/cleavage, cytotoxic, apoptotic, and antibacterial activities of V(IV), Mo(VI), and Ru(II) complexes containing a bioactive ONS-donor chelating agent. *Applied Organometallic Chemistry*, *35*(2), e6082 p.

66. Chen, T., & Wong, Y. S. (2008). Selenocystine induces apoptosis of A375 human melanoma cells by activating ROS-mediated mitochondrial pathway and p53 phosphorylation. *Cellular and Molecular Life Sciences*, *65*(17), 2763.

67. Ferri, K. F., & Kroemer, G. (2001). Organelle-specific initiation of cell death pathways. *Nature Cell Biology*, *3*(11), E255–E263.

68. Reed, J. C. (2001). Apoptosis-regulating proteins as targets for drug discovery. *Trends in Molecular Medicine*, *7*(7), 314–319.

69. Marsden, V. S., O'Connor, L., O'Reilly, L. A., Silke, J., Metcalf, D., Ekert, P. G., Huang, D. C. S., Cecconi, F., Kuida, K., Tomaselli, K. J., Roy, S., Nicholson, D. W., Vaux, D. L., Bouillet, P., Adams, J. M., & Strasser, A. (2002). Apoptosis initiated by Bcl-2-regulated caspase activation independently of the cytochrome c/Apaf-1/caspase-9 apoptosome. *Nature*, *419*(6907), 634–637.

70. Siddiqui, M. A., Alhadlaq, H. A., Ahmad, J., Al-Khedhairy, A. A., Musarrat, J., & Ahamed, M. (2013). Copper oxide nanoparticles induced mitochondria-mediated apoptosis in human hepatocarcinoma cells. *PLOS One*, *8*(8), e69534.

71. Fan, R.-M., Zhu, B.-Z., Huang, C.-P., Sheng, Z.-G., Mao, L., & Li, M.-X. (2016). Different modes of synergistic toxicities between metam/copper (II) and metam/zinc (II) in HepG2 cells: apoptosis vs. necrosis. *Environmental Toxicology*, *31*(12), 1964–1973.

72. Liu, W.-L., Zou, M.-Z., Qin, S.-Y., Cheng, Y.-J., Ma, Y.-H., Sun, Y.-X., & Zhang, X.-Z. (2020). Recent advances of cell membrane-coated nanomaterials for biomedical applications. *Advanced Functional Materials*, *30*(39), 2003559.

73. Gabriella, S., ÁKos, C., Joseph, M., & Leonard, A. (2016). The anticancer activity of the old neuroleptic phenothiazine-type drug thioridazine. *Anticancer Research*, *36*(11), 5701 p.

74. Sharma, P., LaRosa, C., Antwi, J., Govindarajan, R., & Werbovetz, K. A. (2021). Imidazoles as potential anticancer agents: an update on recent studies. Molecules 26, https://doi.org/10.3390/molecules26144213.